

EFFECTS OF HYDROGEN AND ETHYLENE INJECTION SCHEMES IN A
SUPERSONIC AIRSTREAM

By

DANIEL F. CUESTA

A THESIS PRESENTED TO THE GRADUATE SCHOOL
OF THE UNIVERSITY OF FLORIDA IN PARTIAL FULFILLMENT
OF THE REQUIREMENTS FOR THE DEGREE OF
MASTER OF SCIENCE

UNIVERSITY OF FLORIDA

2004

Copyright 2004

by

Daniel F. Cuesta

This document is dedicated to those who dare to dream, carpe diem.

ACKNOWLEDGMENTS

I wish to dedicate this work to the greatest man I have ever known– my father who, by example, has taught me the meaning of hard work, perseverance, sacrifice, and dedication. I would also like to thank my mother for her love, understanding and support. It has allowed me to prosper even in the darkest of times.

This work has benefited from the contribution of many people. The most significant contribution was provided by Professor Corin Segal at the University of Florida. His advice and suggestions have encouraged my continued study in the field of hypersonics. The contributions of Alen Goldman and Paul Ortwerth of the Boeing Corporation also proved invaluable to this work. The assistance of fellow graduate students Nelson Lerma, Jr., Jonas Gustavsson, Amit Thakur and Ron Portz was also helpful.

TABLE OF CONTENTS

	<u>page</u>
ACKNOWLEDGMENTS	iv
LIST OF TABLES	vii
LIST OF FIGURES	viii
ABSTRACT	x
CHAPTER	
1 INTRODUCTION	1
1.1 Introduction.....	1
1.2 Existing Hypersonic Airbreathing Concepts	1
1.2.1 Combined Cycles.....	6
1.2.2 Rocket-Based Combined Cycles (RBCC).....	6
1.2.3 Turbine-Based Combined Cycle (TBCC)	7
1.3 Fuel Choice.....	8
1.4 Developmental Efforts to Date	8
1.5 Previous Work at the University of Florida.....	10
2 EXPERIMENTAL SETUP	12
2.1 Introduction.....	12
2.2 General Facility	12
2.3 Test Section	15
2.4 Injection Schemes.....	17
2.5 Instrumentation and Control	18
3 EXPERIMENTAL RESULTS	24
3.1 Introduction.....	24
3.2 Experimental Conditions and Procedures.....	24
3.3 Configurations	25
3.4 Upstream Injection Penetration and Spreading Calculations	26
3.5 Results.....	28
3.5.1 Effects of Heat Release	28
3.5.2 Comparison of Injection Combinations.....	28
1. Base + Ramp ss vs. Base + Downstream	28
2. Base + Ramp vs. Base + Downstream	30

3. Base + Ramp ss vs. Base + Upstream	31
3.5.3 Comparison of Injection Configuration at Subsonic Conditions	31
1. Upstream + Ethylene Downstream	34
2. Upstream + Downstream vs. Upstream + Ramp.....	34
3. Upstream + Ethylene ramp ss + Downstream vs. Upstream + Ethylene Ramp	34
3.5.4 Fuel Effects.....	35
4 SUMMARY OF RESULTS	37
APPENDIX	
A DATA ACQUISITION AND CONTROL SOURCE CODE	38
B TEST MATRIX.....	45
C HYDROGEN FLOWMETER CALIBRATION.....	46
LIST OF REFERENCES.....	49
BIOGRAPHICAL SKETCH	53

LIST OF TABLES

<u>Table</u>	<u>page</u>
2.1 Discharge coefficients for fuel injection orifices.	18
2.2 Instrumentation specifications.	20
3.1 Outline of experiments performed at Mach 1.6, with hydrogen and ethylene.	25
3.2 Penetration and spreading values at several conditions.	27

LIST OF FIGURES

<u>Figure</u>	<u>page</u>
1.1 Schematic of a 2-D RAMJET. The air enters the diffuser.....	2
1.2 Combustor entrance Mach number versus flight Mach number.....	3
1.3 Schematic of a 2-D SCRAMJET. Air enters the diffuser.....	4
1.4 Approximate specific impulse as a function of Mach number.....	5
1.5 Rocket-Based Combined Cycle (RBCC)-Air is entrained into the engine.....	7
1.6 Turbine-Based Combined Cycle (TBCC).....	8
2.1 Facility Schematic.....	13
2.2 Air-heater/ stagnation chamber schematic.....	14
2.3 Mach 1.6 nozzle and test section schematic.....	16
2.4 Data acquisition and control schematic.....	20
2.5 The facility's air stagnation pressure is controlled by PID.....	22
3.1 Penetration and spreading schematic of upstream fuel injection.....	27
3.2 Pressure rise due to fuel injection in the base + ramp.....	29
3.3 Pressure rise due to fuel injection in the base + downstream.....	29
3.4 Comparison of the ramp ss and downstream injection sites.....	30
3.5 Comparison of the ramp ss and downstream injection sites.....	30
3.6 Ramp ss more efficient than the downstream injection site.....	31
3.7 Downstream and ramp at comparable equivalence ratios.....	32
3.8 At low equivalence ratios, ramp ss and upstream injection sites.....	32
3.9 Upstream interaction was noted at $\phi=0.134$	33

3.10	Ethylene injected in the base at low stagnation pressure.	33
3.11	Ethylene injected downstream and hydrogen injected upstream	34
3.12	Ethylene injected downstream and hydrogen injected upstream	35
3.13	Comparison of downstream vs. ramp ethylene injection	35
3.14	Low stagnation pressure comparison of ethylene injection	36
3.15	Ethylene vs. hydrogen injection with base hydrogen pilot	36

Abstract of Thesis Presented to the Graduate School
of the University of Florida in Partial Fulfillment of the
Requirements for the Degree of Master of Science

EFFECTS OF HYDROGEN AND ETHYLENE INJECTION SCHEMES IN A
SUPERSONIC AIRSTREAM

By

Daniel F. Cuesta

May 2004

Chair: Corin Segal

Major Department: Mechanical and Aerospace Engineering

A study of hydrogen and ethylene combustion was conducted to evaluate various injection schemes in a supersonic airflow at Mach 4.75 flight enthalpy characterized by air stagnation temperature of 900 K and combustion chamber entrance of Mach 1.6. The combination of step and ramp flame-holder was used with fuel injection from four sites—upstream from the step, from the step parallel to the flow, from the base of the step, and downstream of the step. The flame was initiated with hydrogen injection at the base of the step. After this base pilot ignited, the upstream, ramp, and downstream injection occurred according to the pre-defined test matrix. Upon completion of this series, ethylene was tested in a similar fashion. Finally, combinations of hydrogen and ethylene were evaluated with injection in different locations. Equivalence ratios in the range of 0.015 to 0.456 were employed to evaluate wall pressure distribution, injection combination, flame holding and heat release, and stagnation pressure effects. This study

examined the effects of fuel injection location on combustion efficiency. The results indicated the following conclusions:

- Injection into the re-circulation region proved more efficient than alternate schemes due to the ease in mixing with air in this region.
- At low equivalence ratios there was no preferential injection in the combinations tested.
- At high equivalence ratios the supersonic ramp injection was more efficient than the subsonic injection.
- At similar equivalence ratios of about 0.227 the downstream injection and the supersonic ramp yielded a similar pressure rise.
- Upstream interaction is a limiting factor at high equivalence ratios.
- There is a tendency for the pressure rise to reach 2.1 and above at the onset of upstream interaction.
- Upstream injection has a strong tendency to produce upstream interactions when combined with the downstream injection at low equivalence ratios.
- Injection from the supersonic ramp location seemed more efficient than the downstream location at high equivalence ratios.
- At low stagnation pressures, no preferential injection was noted.
- At equivalence ratios above 0.150, ethylene injected through the base produced upstream interactions.

CHAPTER 1 INTRODUCTION

1.1 Introduction

Air based cycles hold the promise of low cost space exploration. Since an air breathing vehicle developed for such an application would not need to carry its oxidizer it could be lighter. It would also operate similar to an airplane, which would simplify ground support needed for launch. Air breathing vehicles may include turbine based cycles (TBCC), or rocket based cycles (RBCC).¹

A major challenge in the development of air breathing hypersonic engines that involve supersonic combustion is efficient mixing and combustion of fuels within a supersonic airstream. This work examines the effect of several fuel injection schemes as well as the combustion efficiency in a supersonic airstream utilizing (i) hydrogen, (ii) ethylene, and an (iii) ethylene-hydrogen combination of fuels.

Reviews by Curran and Murthy¹ include a substantial database of international efforts, some of which are summarized below. Then, a synopsis of the previous, related research conducted at the University of Florida is presented, followed by a description of the intent and scope of this work.

1.2 Existing Hypersonic Airbreathing Concepts

The turbojet engine is limited to operation below Mach 3 due to the high temperature at which the compressor is increasingly exposed as Mach number increases. Because it uses no rotating machinery as turbine engines, the RAMJET can perform at higher Mach numbers.

Figure 1.1 shows a schematic of the RAMJET.² It consists of a diffuser, a combustion chamber and an exhaust nozzle. In the RAMJET, two throats exist. In order for the necessary burner entrance Mach number to be subsonic, the flow is choked downstream, which causes a large backpressure at burner entry. The backpressure thereby induces a oblique shock train ending with a normal shock in the diffuser. Since the stagnation pressure is high, air is compressed in the diffuser to sufficiently high values to achieve an efficient cycle. The air is then mixed with the fuel and burned in the combustion chamber. The hot gases are accelerated in the nozzle. Although the RAMJET can operate at subsonic speeds, it is more efficient at higher flight speeds due to the increased pressure rise upon deceleration of the flow.² The deceleration of the incoming airstream is accomplished by partially supersonic compression through a system of shocks.³ Since the RAMJET cannot operate at Mach 0, it is used in combination with a turbojet or rocket.

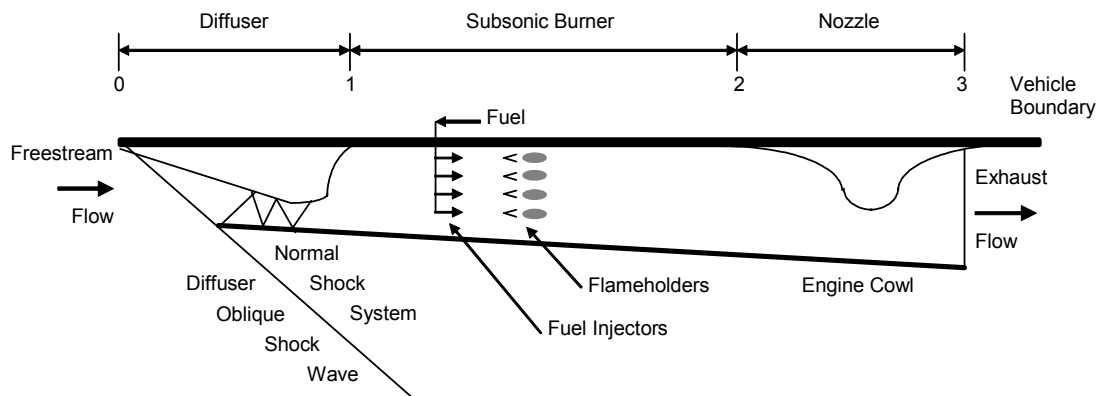


Figure 1.1—Schematic of a 2-D RAMJET.² The air enters the diffuser where a shock system decelerates the flow to subsonic speeds before entering the burner.

For flight speeds exceeding the Mach 5 to 6, it becomes impractical to decelerate the flow to subsonic velocities due to several problems⁴ including:

- a. High static temperature leading to dissociation therefore preventing efficient heat release through recombination reactions.
- b. Significant pressure losses induced by normal shocks.

Analyses show that the combustor inlet temperature should be within the range of 1400 – 1700 K.⁵ Using data from the standard atmosphere⁶ and taking the representative temperature as 1600 K, Figure 1.2 shows combustor entrance Mach number for flight at different altitudes.² As flight Mach number increases, the combustor entrance Mach number increases as well, exceeding Mach 1. Upon reaching a flight Mach number of around Mach 6 it becomes practical to maintain supersonic combustor flow. This type of engine is called a supersonic combusting RAMJET or SCRAMJET.

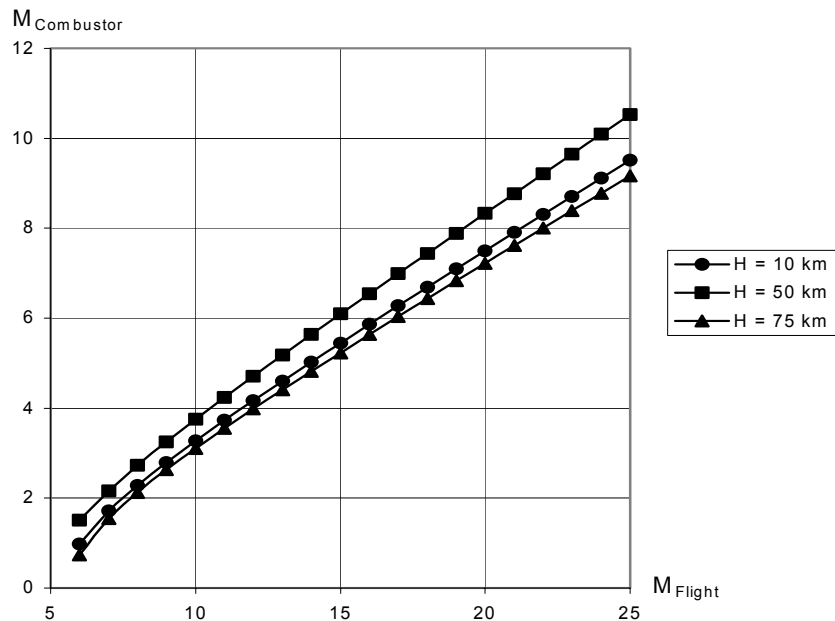


Figure 1.2—Combustor entrance Mach number versus flight Mach number for different altitudes ($\gamma = 1.4$, $T_1 = 1600 \text{ K}$)²

Figure 1.3 shows a schematic of a SCRAMJET engine.² As the flow enters the diffuser from the left it passes through an oblique shockwave, which decelerates the flow

slightly as it enters the burner still at supersonic speeds. The presence of an oblique shock train upstream of the combustor provides the necessary adiabatic pressure rise to counteract the pressure rise from heat addition in the combustor, and thus preventing unstart of the inlet.

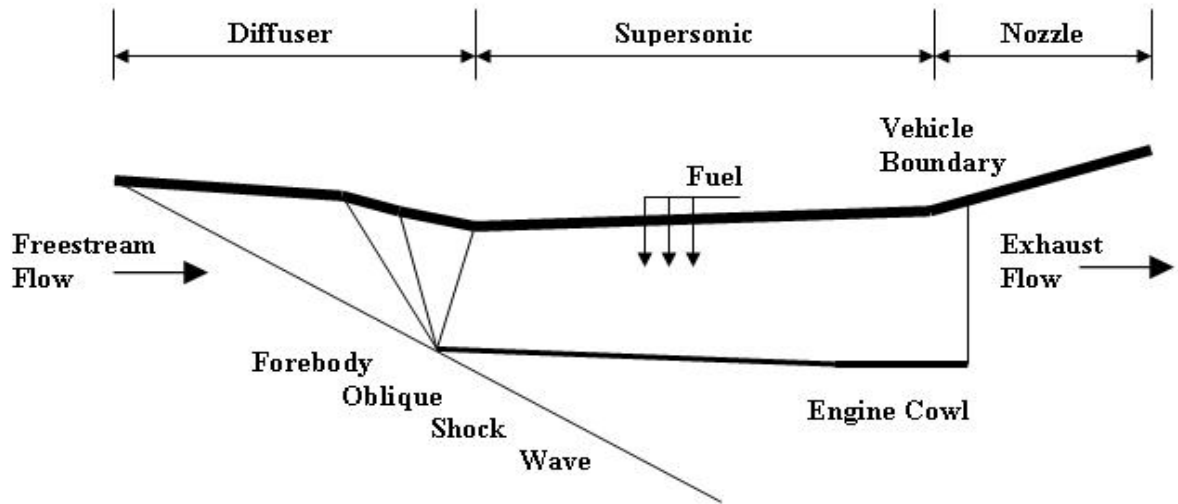


Figure 1.3—Schematic of a 2-D SCRAMJET² Air enters the diffuser where an oblique shock system decelerates the flow slightly to enter the burner at supersonic speed where it is burned.

A significant parameter characterizing an engine's efficiency is the fuel-specific impulse defined as:

$$I_P = \frac{\text{uninstalled thrust}}{\text{fuel weight flowrate}} = \frac{F}{g\dot{m}_p} \quad \text{Eq. 1.1}$$

The fuel-specific impulse is the ratio of an engine's thrust to weight of fuel burned in one second. Figure 1.4 shows the specific impulse for various propulsion systems. It can be seen that for flight Mach numbers greater than 6, the SCRAMJET specific impulse is superior to that of the RAMJET.¹

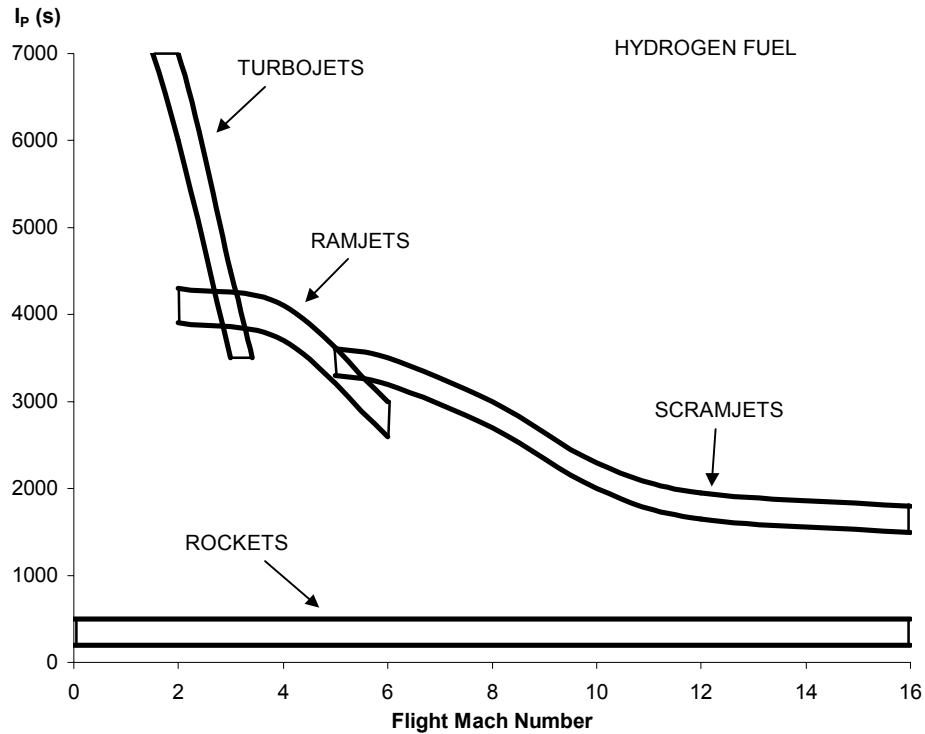


Figure 1.4—Approximate specific impulse as a function of Mach number for various mode of aerospace hydrogen-based propulsion.¹

The difficulties surrounding the SCRAMJET technology are multiple. First and foremost is the timescale of combustion. The residence time is considerably shorter in a SCRAMJET engine becoming comparable with the combustion time.⁷ In order to efficiently burn the fuel in the combustor, a suitable injection scheme must be developed that achieves fast mixing and combustion.

Different fuels have been proposed taking into account such properties as density, weight, and volatility.⁸⁻¹⁰ Hydrogen fuel has fast chemical reactions when compared with hydrocarbons.^{7,11,12} It has, however, low density requiring a large volume and therefore increasing the fuel tank size adding more weight to the vehicle. Hydrocarbon fuel combustion is addressed in detail in Ref. 13.

1.2.1 Combined Cycles

Due to RAMJET and SCRAMJET inability to function at subsonic Mach numbers an array of variations have been conceived. Of these ideas, the Dual-Mode Combustion System,^{14,15} Rocket-Based Combined Cycle (RBCC),¹ and Turbine-Based Combined Cycle (TBCC)¹ attract most attention.

The requirements of high efficiency and the dissociation of air at high static temperatures dictate that combustion must take place at subsonic speeds for the RAMJET and supersonic speeds for the SCRAMJET.¹ To avoid having two entirely different engines it is desired to operate an engine in a dual mode, i.e. in RAMJET and then, upon reaching Mach 4 to 5, SCRAMJET mode. A synergistic approach is achieved by combining the turbine or the rocket cycle with the RAMJET-SCRAMJET cycle. A thorough analysis of the dual-mode combustion system can be found in Ref 14, 15, and 16.

1.2.2 Rocket-Based Combined Cycles (RBCC)

The RBCC configuration consists of four different operating modes- ejector, RAMJET, SCRAMJET, and rocket mode.¹⁷ A schematic of a RBCC is presented in Figure 1.5. The ejector mode is a pumping device, which exchanges momentum between a high-speed primary fluid and a low speed secondary fluid to produce an increased mass flow rate in the secondary flow. The secondary flow would be the incoming airstream. The primary fluid would be rocket exhaust gases. The ejector mode would propel the air-breathing vehicle from static to Mach 2. After the ejector mode operation, the vehicle would transition into a RAMJET mode and SCRAMJET mode, respectively. Finally, as

the vehicle enters the upper atmosphere where the oxygen is insufficient to sustain combustion, the transition back to rocket mode would occur.

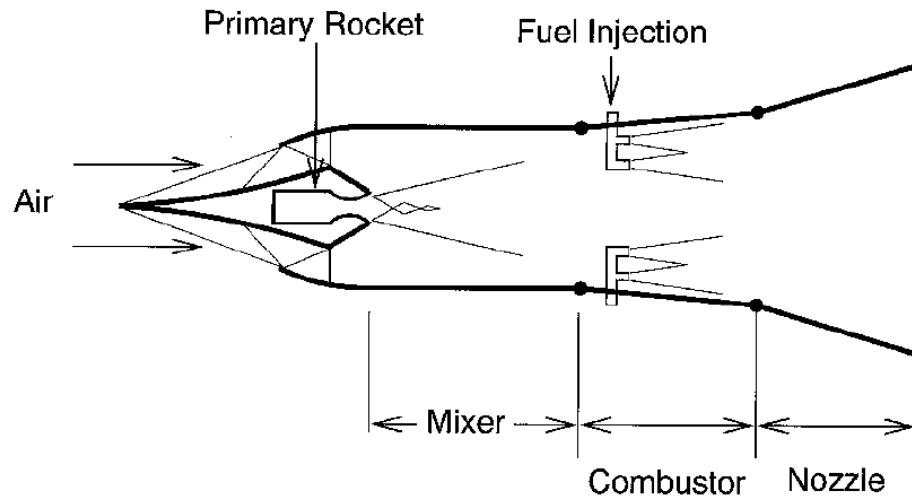


Figure 1.5–Rocket-Based Combined Cycle (RBCC)-Air is entrained into the engine by the rocket from the left. It is then mixed with fuel and burned in the combustor.¹⁸

1.2.3 Turbine-Based Combined Cycle (TBCC)

Figure 1.6 shows a schematic of a TBCC. The TBCC would operate just as the RBCC with the exception that instead of the first mode being a rocket, it would be a turbine-compressor system. The major drawback would be that the transition from the turbine-compressor mode to RAMJET would require substantial geometry changes, increasing the vehicle weight.¹

Several configurations have been evaluated.¹⁵ Among them, a study of podded air-turbo rockets (ATR) installations using variable geometry supersonic through-flow fans (STFF) has demonstrated gains in performance over conventional ATR-RAMJET concepts.¹⁹ The simplicity of the STFF contributes less weight to the vehicle. Although this technology seems viable more work needs to be done to improve its efficiency.

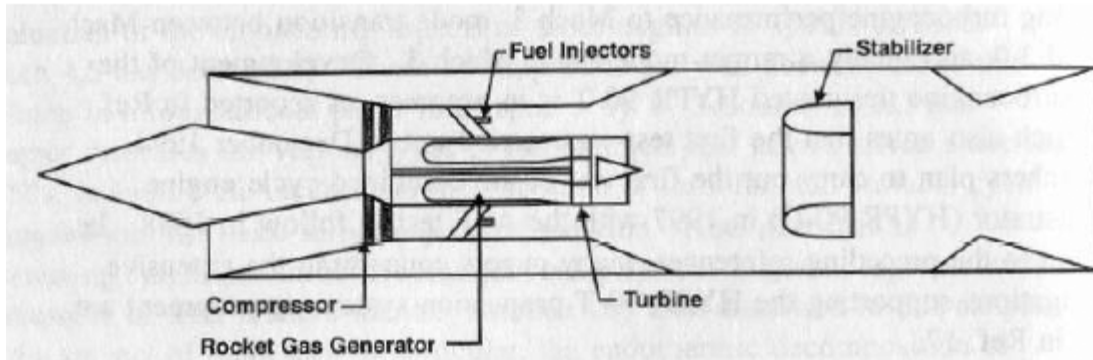


Figure 1.6–Turbine-Based Combined Cycle (TBCC)-Air is entrained into the engine by the turbine from the left. It is then mixed with fuel and burned in the combustor.²⁰

1.3 Fuel Choice

In order for the SCRAMJET concept to function properly an efficient balance between fuel mixing, combustion efficiency and injection schemes must be achieved. The fuel selection has been investigated in many experiments to date.^{21–25} JP type fuels are preferred over the faster burning hydrogen due to their higher density and corresponding reduced tank volume.²⁴ Furthermore, the ease of handling and increased safety is more attractive for intermediate range applications, to Mach 8. Hydrocarbon fuels such as JP fuels were shown to reach an upper bound flight Mach number between Mach 9 and 10.²⁴ Studies of the stability of hydrogen and hydrocarbon blended fuels were conducted and compared with analytical data.^{7,25} Other suggested fuels were hydrogen peroxide, kerosene^{26,27} and methane. In Ref. 28, it was noted that methane provided the maximum range performance due to its high density and high specific energy content.

1.4 Developmental Efforts to Date

The major current U.S. led efforts are the joint NASA/Air Force Hyper-X (X-43A) program, and the slightly larger X-43C. The X-43A is designed to provide only a

few seconds of flight with heat sink hardware. The X-43C project intends to achieve flight demonstration of the USAF HyTech engine, which is a dual-mode scramjet.¹⁵ The X-43 will be a multiple engine module, vehicle capable of Mach 5 to 7 flights. It will utilize JP-7 fuel for active regenerative fuel cooling to the engine.¹⁵

Ref. 29 describes an injection scheme suggested by Russian researchers that includes strut injectors along with a downstream cavity incorporated into a dual-mode SCRAMJET test model (DMSCRAM). Low combustion efficiency was noted due to the non-uniform distribution of fuel between injection sites on the struts. Duct geometries were also investigated with varying wall inclination angles.³⁰ These experiments showed the effect of flow separation on the supersonic airstream.

Japan experimented with an array of struts and steps at different angles in order to increase the pressure in the combustor section and for better combustion performance.³¹ Fuel injection was performed transverse and parallel to the airflow. Results are tabulated in Ref. 31.

Australia has launched a scramjet in July of 2002. The program, called HYSHOT, demonstrated supersonic combustion but did not obtain positive thrust.³² The program utilized wall injection, a central injection configuration and port injection.³³ Experiments are performed in a T-4 shock tunnel capable of producing flows up to 6 km/s and a Mach 3 small supersonic blow down tunnel.

Germany has investigated various methods of injection from fins and tubes to struts and wedges.³⁷ Combustion efficiency seemed preferential to ramp and tube injection.

The issue of injection configuration selection that will ensure efficient mixing and combustion continues to remain a subject of great interest.

1.5 Previous Work at the University of Florida

A study conducted by Owens²⁷ evaluated combustion efficiencies for pre-heated kerosene in the presence of a hydrogen pilot injected parallel to the air stream for several injection configurations. The injection configurations included (i) a generic, rearward-facing step, (ii) a modified rearward-facing step with beveled edges to facilitate vortex enhanced mixing, and a rearward-facing step to serve as an additional flame-holder for liquid kerosene. The results indicated when the beveled step was used, the highest combustion efficiency (64%) was observed due to enhanced mixing in the far field.²⁷ At low hydrogen-pilot equivalence ratios (0.02), the kerosene combustion efficiency was approximately 60%. The baseline configuration with the generic step yielded an efficiency of 57% with a tendency to decrease as the hydrogen pilot was increased past an equivalence ratio of 0.028.

A subsequent study was performed to examine the stability of a flame in the re-circulation region with injection of kerosene upstream of the region.³⁵ A hydrogen pilot was used with injection parallel to the flow into the re-circulation region and several cavities for flame-holding. Geometry changes have shown a small effect on the flame stability in the re-circulation region. The injection of hydrogen at high flow rates into the re-circulation region resulted in increased size and thereby entrains more air in the re-circulation region to accomplish a more stable combustion. The injection of kerosene upstream of the re-circulation region proved detrimental to combustion efficiency. The rich boundary layer arriving into the re-circulation region resulted in rich mixtures and extinguished the flame.

Analysis of thermal choking effects was conducted in Ref.36. The performance of a combined hydrogen fuel injection scheme was evaluated between two injection zones. The results indicated that at low total equivalence ratios (approx. $\phi = 0.35$), no preferential injection mode exhibited superior efficiency. However, at large total equivalence ratio, injection through the base produced a larger pressure rise as a result of an increased residence time in comparison with the ramp injection. It was noted that within the constant area of the combustion chamber, the slow speed burning layer that begins at the base of the flame-holder creates a combustor blockage that takes the shape of a convergent-divergent channel. Therefore, the maximum pressure rise occurs in the middle of the constant area duct, and the core flow accelerates in the divergent part. This favorable pressure gradient tends to decrease the shear layer growth. Within the range of $\phi = 0.1 - 0.5$ the transition from near complete combustion to lower combustion efficiency occurred, with efficiency decreasing at higher equivalence ratios.

Residence time of the fuel can be increased by (i) flow path geometries, (ii) injection configuration, and (iii) injection port combinations.¹⁷⁻²¹ This work examines the efficiency of some potential solutions. Continuing the study from Ref. 36, the current work evaluated combinations of injection configurations. The efficiency was determined through the pressure rise in the combustor as a result of heat release.

CHAPTER 2 EXPERIMENTAL SETUP

2.1 Introduction

This project utilized the existing SCRAMJET facility at the University of Florida described in detail by Michael Owens.² A liquid fuel heater, fuel mass flowmeters, and zirconia coating inside the combustion chamber were modifications that expanded and improved the facility. This chapter describes the facility, test section, injection configuration, instrumentation and control.

2.2 General Facility

The University of Florida scramjet facility operates with air stagnation temperature up to 1200 K and stagnation pressure up to 10 atmospheres. A vitiated heater is utilized to maintain hypersonic flight enthalpy during the experiment. Interchangeable nozzles produce test section Mach numbers from subsonic to Mach 3.6. Figure 2.1 shows a schematic of the general facility.

Hydrogen is supplied to the vitiated air heater from a H₂ tank farm. Oxygen consumed during the hydrogen combustion is replaced from an O₂ tank farm that feeds into the incoming air prior to hydrogen combustion. Therefore, hydrogen combustion occurs in oxygen enriched air leaving the heater with a constant 0.21 oxygen mole fraction at all conditions and constant stagnation temperature at the exit. The vitiation with water may affect the chemical reactions in the test section. During these tests the stagnation temperature was limited to 900 K resulting in a low level of vitiation. This process is controlled by a fuzzy logic controller developed in LabVIEW by Owens.²

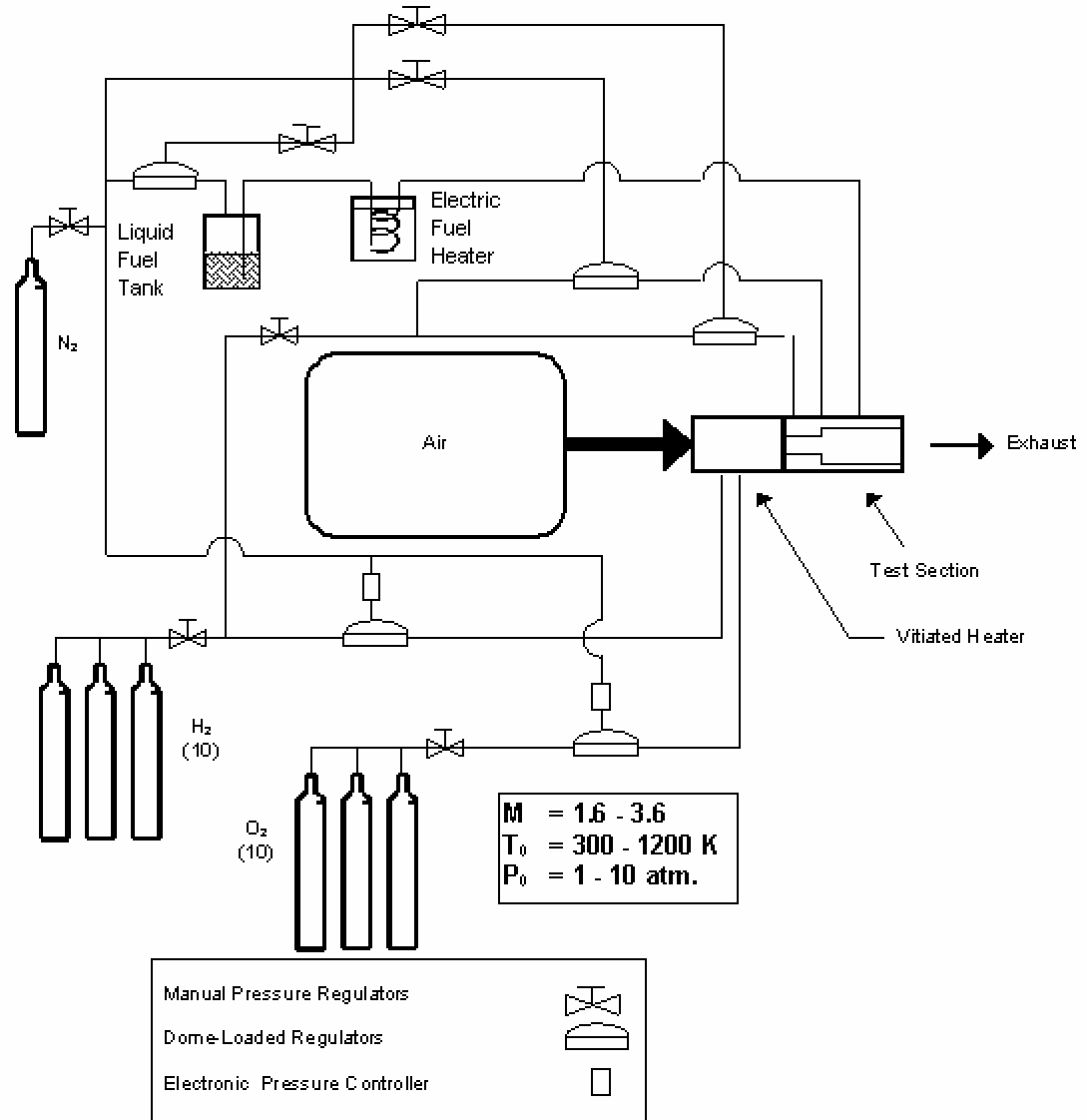


Figure 2.1- Facility Schematic

Two porous plugs and eight sonic air jets are incorporated into the heater/stagnation chamber to improve mixing and provide a uniform stagnation temperature distribution. The eight air jets, two sets of four, are placed equidistant from each other in an annular fashion in the vitiated heater. Their purpose is to entrain colder air into the higher temperature core flow. One set of air jets are slightly offset in order to add swirl

to the flow as seen in the Figure 2.2. At the exit of the heater two porous plugs further help removing the thermal gradients.

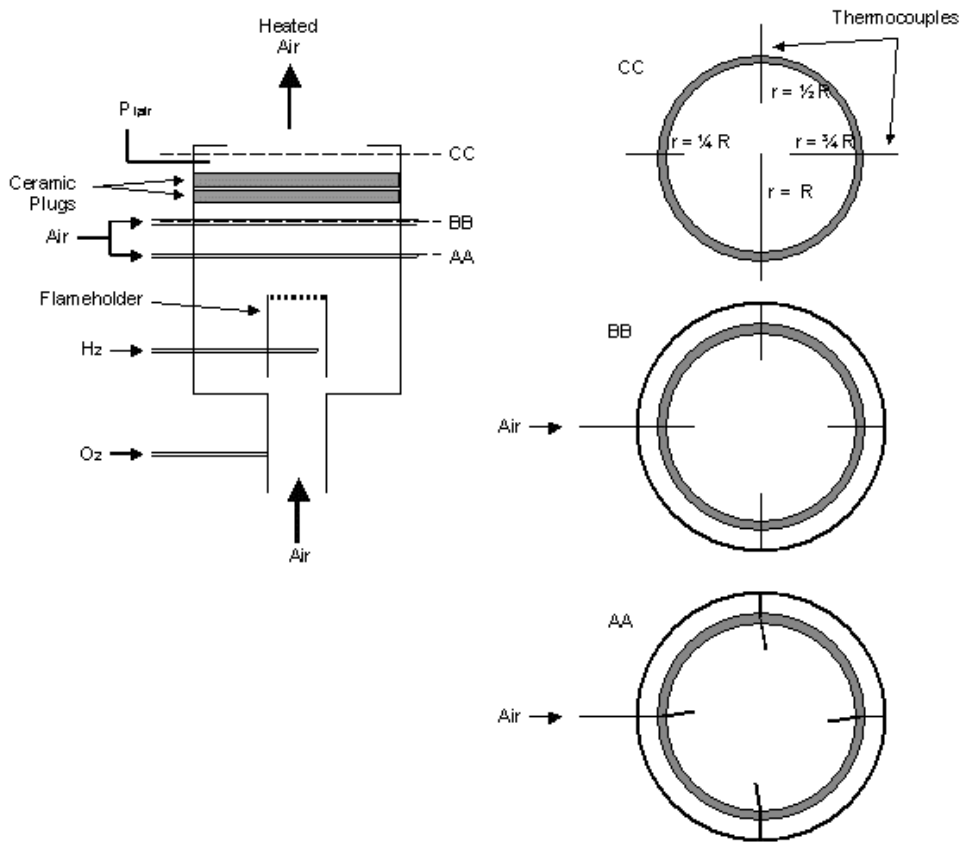


Figure 2.2- Air-heater/ stagnation chamber schematic

The air-heater / stagnation chamber is equipped with pressure transducers and thermocouples to provide the air stagnation temperature and air stagnation pressure. Properties of the air are measured at the exit of the chamber downstream of the ceramic plugs. Air stagnation temperature is taken to be an area weighted average of four thermocouples spaced at four radial locations in the exit plane of the chamber also shown in Figure 2.2. The calculation is given by:

$$T_{air,t} = 0.0152T\left(\frac{r}{R} = 1\right) + 0.1222T\left(\frac{r}{R} = \frac{3}{4}\right) + 0.2444T\left(\frac{r}{R} = \frac{1}{2}\right) + 0.6181T\left(\frac{r}{R} = \frac{1}{4}\right)$$

Eq. 2.1

Wall pressure is measured at two locations for safety. The heater inner wall is covered with a 0.5 cm thick layer of aluminum oxide ceramic putty for thermal insulation.

Upon exiting the vitiated heater, the flow goes through the bell mouth with compression on four sides to a 2-D rectangular supersonic nozzle. Six interchangeable, supersonic nozzles are available allowing the entrance Mach number to the test section to be varied from 1.6 to 3.6. Each nozzle has a fixed exit area of 2.54-cm by 2.54-cm. The nozzles are equipped with a pressure port to measure the freestream static pressure at the nozzle exit.

An isolator follows to prevent shocks propagating upstream. Downstream of the isolator, a 2.54 cm collar contains the upstream fuel injection ports. Finally, the flow enters the combustion chamber described below.

2.3 Test Section

The test section is composed of the isolator, isolator collar, and combustion chamber as shown in Fig. 2.3. Air exits the supersonic nozzle at the selected Mach number and enters the isolator, a 2.54 cm by 2.54 cm cross section, 15 cm long. The conditions at the isolator entrance are taken to be freestream conditions. Next, the flow enters the isolator collar which has the same cross section and is only 2.54 cm in length. Its purpose is to provide a location for upstream injection. The upstream injection location is placed at $-4H$ with H , the step height equal to 1.25 cm. This location was selected to achieve a desired fuel penetration and spreading as described below. The test section uses a ramp configuration with antisymmetric geometry on the opposite side. From these steps two injection sites are available followed by additional injection ports in the test section walls.

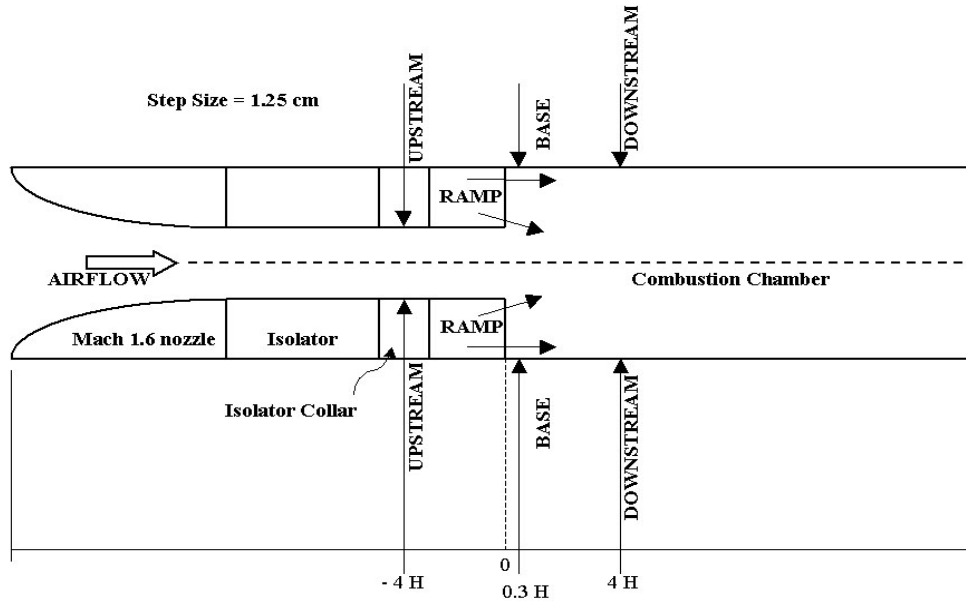


Figure 2.3-Mach 1.6 nozzle and test section schematic. Airflow enters the nozzle from the left side.

Behind the steps the recirculation region provides the main flame holding mechanism. The base injection site consists of nine holes each of 0.05 cm diameter. Further downstream injectors are present at $2.4H$ and $4.0H$. After the ramps, the combustion chamber follows as a constant 2.54 by 5.00 cm rectangular duct for 33 cm in length.

Visual access to the test section is provided by quartz windows installed at the entrance region of the test section. The test section incorporates eight pressure ports on each side. Additionally, five thermocouples are embedded on each side of the test section wall at 0.1 mm below the wetted surface. Fuel pressure is measured with transducers placed in the supply lines. Two Asco FTP-900 flowmeters are available to measure fuel mass flow rates. Their description and calibration is included in Appendix C.

The combustion chamber and ramp faces are coated with a 0.33 mm thick zirconia layer coating in order to maintain higher temperatures inside the chamber. An active

cooling system is incorporated so that no damage to the hardware will occur during experiments when the windows are replaced with blanks made of brass.

2.4 Injection Schemes

Fuel was injected in three main areas: upstream of the step at $-4H$, in the base of the step, and downstream of the step at $4H$. The upstream injector is designed to provide partial premixing before reaching the test section entrance. Calculation of spreading and penetration for the upstream injection site was based on correlations obtained in previous work by Hojnacki.⁴² Using these correlations injection diameters and location were selected to obtain a certain degree of premixing. The results of these calculations are presented in chapter 3. The purpose of the analysis lies in the fact that a stoichiometric or near stoichiometric fuel/air ratio is desired at the entrance to the combustor.

At the base injection site after the step, three forms of injection were employed:

- Nine orifices of 0.50 cm diameter transverse to the flow located at the entrance to the combustion chamber, at $0.5H$ from the step.
- From the step in an axial direction to the flow from five orifices. Three orifices evenly spaced at the base of the step are 0.08 cm in diameter and two orifices of 0.05 cm in diameter. Their total effective area is 0.035 cm^2 .
- Supersonic nozzle injection facing slightly offset to the axis of flow into the center of the flow field with a diameter of 0.17 cm.

A sonic downstream injection site exists downstream of the step at $2.4H$ and $4H$. An orifice on each side of 0.15 cm diameter was utilized for injection in this case at $4H$. The discharge coefficients of all fuel injection orifices are presented in Table 2.1.

Table 2.1 Discharge coefficients for fuel injection orifices.

<i>Injector</i>	<i>Mode of injection</i>	C_d	<i>Hole diameter d mm (in)</i>	<i>No of holes N</i>
Isolator	transverse	0.82	0.51 (0.020)	4
Base	transverse	0.91	0.51 (0.020)	10
Generic ramp*	parallel	0.71	0.76 (0.030)	18
Ramp (nozzle holes)	parallel	0.70	1.73 (0.068)	4
Ramp (small holes)	parallel	0.90	0.51 (0.020)	4
			0.76 (0.030)	6
Downstream (1.0 mm)	transverse	0.78	1.02 (0.040)	2
Downstream (1.5 mm)	transverse	0.79	1.52 (0.060)	2

* Not used in this study

2.5 Instrumentation and Control

Figure 2.4 shows a schematic of the data acquisition and control (DAQC) hardware. The DAQC hardware consists of the instrumentation installed on the facility and the computer hardware used to acquire and / or output instrumentation signals.

The computer hardware for acquiring / output of the instrumentation signals consists of:

1. A 1.4-GHz Pentium based computer.
2. A National Instruments AT-MIO-16E-2 data acquisition board installed in the computer, featuring 8 differential input channels and a 500 kHz maximum scan rate.
3. A National Instruments SCXI-1000 chassis / SCXI-1100 multiplexer / amplifier combination cabled to the AT-MIO-16E-2 data acquisition board.
4. An RS-232 serial port installed in the computer.
5. A National Instruments PCII/IIA GPIB interface board installed in the computer.

Instrumentation signals are acquired from six types of devices:

1. Four Omega TX303 absolute pressure transducers generating 0.5 to 5.5-volt signals that are proportional to the pressure sensed and are read via the AT-MIO-16E-2 data acquisition board.
2. Twelve Omega k-type thermocouples generating voltage signals that are a polynomial function of junction temperature and are read by the AT-MIO-16E-2 / SCXI combination.
3. One Sponsler MF30 turbine flowmeter generating a 0 – 2200 Hz signal that is proportional to the volumetric flow rate and is read by the AT-MIO-16E-2 data acquisition board.
4. A Pressure Systems PSI-9010 pressure scanner featuring a bank of 16 gage-pressure transducers that is read via the RS-232 serial port.
5. A Mensor DPG II 200-psia absolute pressure transducer that is read via the PCII/IIA GPIB interface board.
6. Two Omega FTB-900 flowmeter read via AT-MIO-16E-2/ SCXI combination.

Details on the specific devices are given in Table 2.2. Additionally, set point voltages are output to two Tescom ER-3000 electronic PID controllers. The air stagnation pressure is read by the Mensor DPG II pressure transducer. The air static pressure at the nozzle exit and the test section wall pressures are measured by the Pressure Systems PSI 9010 pressure scanner. The H₂ and O₂ stagnation pressures in the air-heater and the fuel pressures are each measured by an Omega PX303 200-psia pressure transducer.

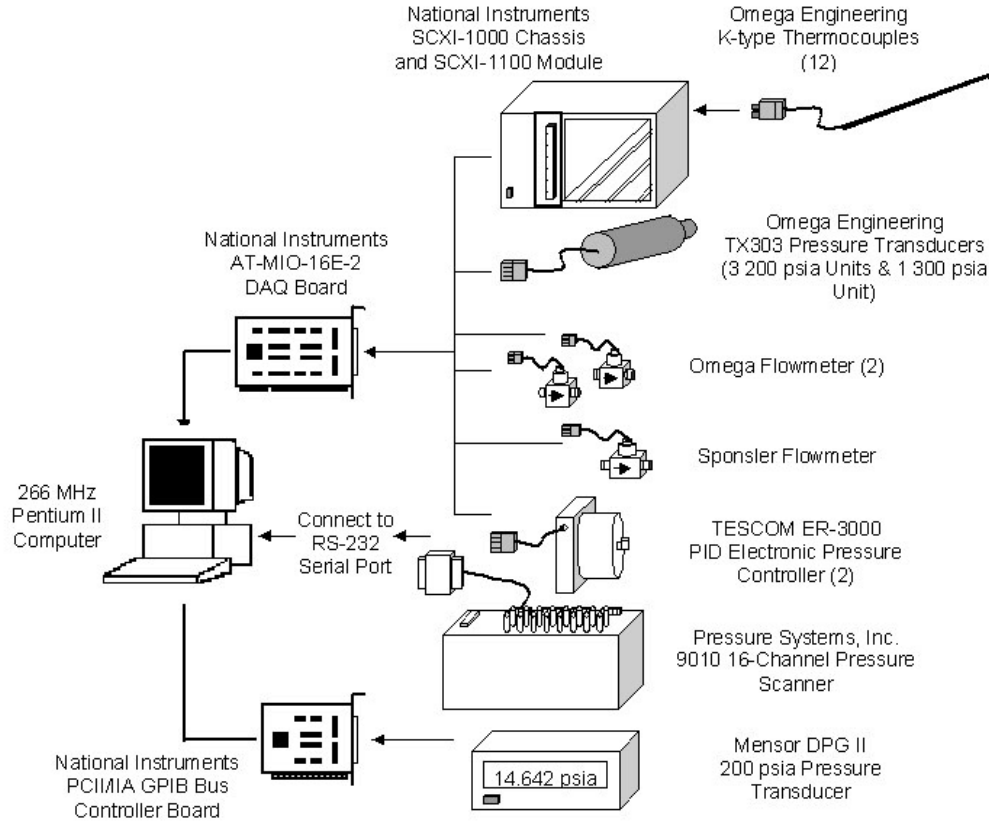


Figure 2.4– Data acquisition and control schematic.

Table 2.2– Instrumentation specifications

Manufacturer and Model	Measurand Sensed	Controlled	Range	Input	Output	Feedback
Pressure Systems PSI 9010 Pressure Scanner	$P_{air}, P_w \left(\frac{x}{H} \right)$		307 kPa (0 – 30 psig)		PC Serial Port	
Omega Engineering PX300 Pressure Transducer	$P_{t,H2}, P_{t,O2}$ $P_{t,H2-pilot}, P_{t,K}$		1379 kPa (0 – 200 psia)		1 – 5 V analog	

Table 2.2- Continued

Omega Engineering K-Type Thermocouple	$T_{t,air}, T_{t,K}$ $T_W \left(\frac{x}{H} \right)$		300 – 2000 K		0 – 50 nV analog	
Mensor DPG II Pressure Transducer	$P_{t,air}$		1379 kPa (0 – 200 psia)		PC GPIB Board	
Tescom ER-3000 Electronic Pressure Controller		Tescom 4400		0.5 – 5.5 V analog	689.4 kPa (0 – 100) psig N ₂	0.5 – 5.5 V analog
Tescom 4400 Series Dome-Loaded Pressure Regulator		P_{t,H_2}, P_{t,O_2} $P_{t,H_2-pilot}, P_{t,K}$		414 kPa (0 – 60 psig) N ₂	4136 kPa (0 – 600 psig) H ₂ , N ₂ , or O ₂	
Tescom 1300 Series Manual Pressure Regulator		Tescom 4400		Manual Operation	689 kPa (0 – 100 psig) N ₂	
Ametek PMT Model 40 Pneumatic Controller		Fisher Model ED		Dial Selectable	307 kPa (0 – 30 psig) N ₂	1039 kPa (0 – 150 psig)
Fisher Controls Type ED Dome-loaded Butterfly Valve		$P_{t,air}$		2068 kPa (0 – 300 psig)		
National Instruments AT-MIO-16-E2 DAQ Board				±10 V analog (8)	±10 V analog (2)	
National Instruments PC II/IIa GPIB Controller Board		Mensor DPG II Pressure Transducer				
Omega FTB-900 Flowmeter (2)	\dot{m}_{fuel}		0-2000 Hz	12 – 28 V	4 – 20 mA	

Omega K-type thermocouples are used to measure the four temperatures used to determine the air stagnation temperature, the two air-heater wall temperatures, the kerosene fuel temperature, and the five per side test section wall temperatures.

The facility incorporated both manual and automated control. Figure 2.5 shows a schematic of the facility control apparatus. The air stagnation pressure is controlled by a combination of a Fisher Type ED dome-loaded butterfly valve and an Ametek PMT Model 40 pneumatic PID pressure controller. The valve position is a function of the pressure supplied to the dome. The dome pressure is modulated by the pneumatic PID pressure controller to achieve the desired air stagnation pressure. The pneumatic PID controller features a manual, dial set point.

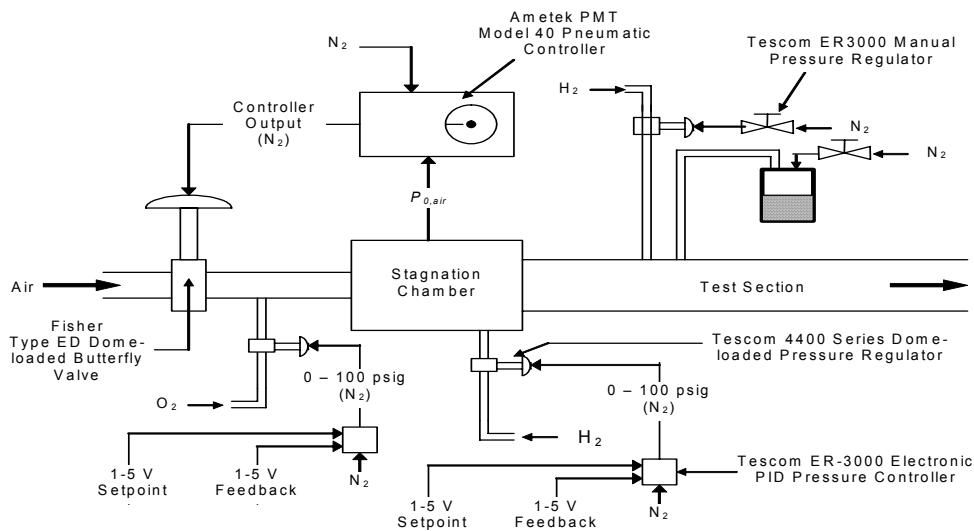


Figure 2.5-The facility's air stagnation pressure is controlled by PID controller and a dome-loaded butterfly valve.

The control scheme has been described in detail elsewhere.² Both the H_2 and O_2 stagnation pressures in the air-heater are each controlled by a combination of a Tescom 4400 Series dome-loaded pressure regulator and a Tescom ER-3000 electronic PID pressure controller. The dome-loaded pressure regulators provide an output pressure that is ten times the pressure supplied to the dome. The electronic PID pressure controllers

receive an analog set point from the DAQ board installed in the computer and modulate the dome pressures to achieve the desired H₂ or O₂ pressure. The set points for the electronic PID controllers are determined by a LabVIEW program that is described in the following chapter.

Both the pilot H₂ and the other fuels are controlled by a manually operated Tescom 1300 Series pressure regulator in combination with a Tescom 4400 Series dome-loaded pressure regulator. The manual pressure regulators provide a user determined pressure to the dome-loaded pressure regulators thus achieving the required fuel pressure

CHAPTER 3 EXPERIMENTAL RESULTS

3.1 Introduction

Experiments that examined the efficiency of using several fuels, injection configurations and stagnation pressures in a Mach 1.6 airflow were conducted. Three different fuels- hydrogen, ethylene, and a combination of both at high and low stagnation pressures were injected into the supersonic airflow at the Upstream, Base, Ramp, and Downstream locations.

The specific effects investigated were:

1. Investigation of heat release features of selected configurations via wall pressure distribution in the isolator and combustion chamber.
2. Effects of heat release at subsonic flow conditions.

This chapter presents the result of these investigations. The configurations, conditions, and procedures are initially discussed, followed by a discussion on the penetration and spreading of the upstream fuel injection. Analysis of the tests follow and the conclusions drawn from the experimental results are then summarized.

3.2 Experimental Conditions and Procedures

A list of experimental conditions conducted is presented in Appendix B. All supersonic experiments were conducted at combustor entrance $M=1.6$, with nominal stagnation temperatures of 900 K, and stagnation pressures up to 483 kPa (65 psia). For subsonic experiments the stagnation pressure was lowered to unstart the combustion

chamber. Fuel temperatures were kept at 300 K before injection. Table 3.1 presents an outline of the analyses presented in the following section.

Experiments began with the heating of air in the vitiated heater, or ramp up.² As the stagnation temperature reached the set point value of 900 K, a pilot flame was ignited in the base in most cases. Then additional fuel was injected according to the goals of the experiment and throttled to a desired value. Video was acquired in most experiments to determine the quality of the flame. For ethylene combustion dichroic color filters were used to reduce the bright emission from the ethylene flame, thereby revealing more flow features.

Table 3.1- Outline of experiments performed at Mach 1.6, with hydrogen and ethylene fuel.

Investigation	Fuels					
	hydrogen		ethylene		hydrogen & ethylene	
	Configuration	Test	Configuration	Test	Configuration	Test
I. Heat release effects	1. Base + Ramp(Supersonic) 2. Base + Downstream	5-19-03-A 5-21-03-A				
II. Comparison of injection combinations with hydrogen	1. Base + Ramp(Supersonic) vs. Base + Downstream Upstream + Ramp 2. Base + Ramp vs. Upstream + Base 3. Base + Downstream vs. Ramp + Base	5-19-03-A 5-21-03-A 5-16-03-B 6-5-03-A 4-7-03-A 6-4-03-A 6-5-03-A				
III. Comparison of injection configuration with ethylene			1. Upstream + Base + Downstream Base and Downstream 2. Upstream + Base + Ramp Base and Downstream	7-17-03-C 7-17-03-A 7-21-03-B 7-17-03-A		
IV. Subsonic operation					1. Upstream + Downstream Upstream + Downstream 2. Upstream + Ramp Upstream + Downstream 3. Upstream + Ramp Upstream + Base + Downstream	7-8-03-A 7-8-03-C 7-8-03-B 7-8-03-C 7-8-03-B 7-23-03-B
						6-11-03-A

3.3 Configurations

Injection was performed from four injection sites upstream, ramp, base, and downstream. Figure 2.3 shows the injection site locations. Injection was accomplished perpendicular to the airflow at the Upstream, Base, and Downstream sites. Parallel

injection was performed through sonic or supersonic orifices located at the Ramp site.

The ramp site contained two different modes of injection. The first mode contained five orifices of different diameters with an effective area of 0.035 cm². Sonic injection

through these orifices occurred at the base of the step, parallel to the flow at 0.5 H above

the test section wall. The second mode offered by the ramp site is supersonic injection

through two holes of 1.7 cm in diameter on each side. In order to distinguish between the

two injection modes in the ramp, the supersonic injection was named 'Ramp ss'.

Transverse base injection occurs at 0.5H, after the step. It is used as a pilot for several

tests in particular when direct ignition is difficult to achieve. The downstream injection

follows at 2.4H after the step in the combustor.

3.4 Upstream Injection Penetration and Spreading Calculations

Upstream fuel injection, was used to obtain a stoichiometric ratio of approximately 0.068 at the entrance to the combustor. To achieve this value, the orifice size and

distance upstream of the ramp was determined according to the calculations by

Hojnacki.⁴² The equations used are as follows:

$$\frac{x}{d_0} = 4.45 \times \left(\frac{\rho_{\text{fuel}}}{\rho_{\text{air}}}\right)^{0.5} \times \left(\frac{V_{\text{fuel}}}{V_{\text{air}}}\right) \times \left(\frac{z}{d_0}\right)^{0.27} \quad \text{Eq. 3.1}$$

$$\frac{y}{d_0} = 6.95 \times \left(\frac{z}{d_0}\right)^{0.33} \quad \text{Eq. 3.2}$$

where the values of x_0 and z_0 are penetration and spreading, respectively and d_0 is the orifice diameter. The distance z is the length required to fill up half of the isolator

cross section with fuel upon entering the combustor as shown in Figure 3.2. A

spreadsheet was constructed for various orifice diameters and stoichiometric ratios to

determine the optimum upstream location for the different fuels. The results are tabulated in Table 3.2.

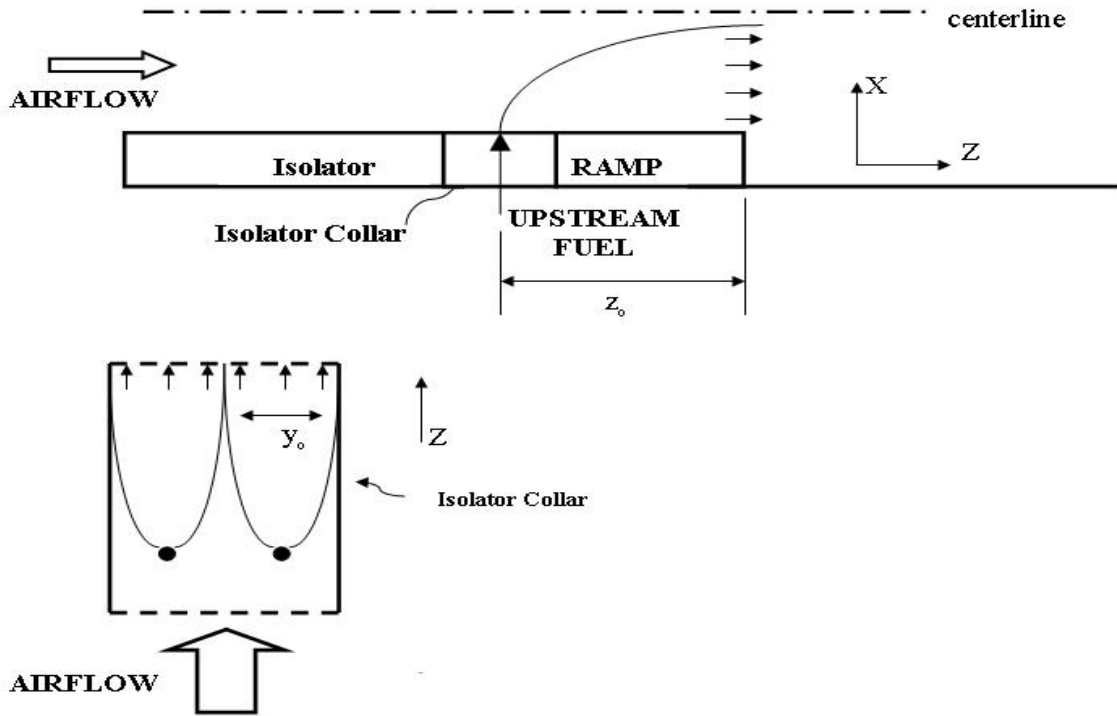


Figure 3.1-Penetration and spreading schematic of upstream fuel injection.

From this calculation two orifices on each side were selected equally placed in a cross section direction. The diameter was 0.5 mm and resulted in a penetration of 67% of the duct height and a spreading of 64% of the width. At the combustion chamber entrance, $\phi = 0.09$ for hydrogen.

Table 3.2 -Penetration and spreading values at several conditions.

distance z cm (inches)	x/d0	y/d0	Orifice diameter cm (in)	f/a	1 injector	2 injectors
3.30 (1.3)	29.67	27.56	0.051 (0.02)	0.0017	0.057	0.113
3.56 (1.4)	30.27	28.24	0.051 (0.02)	0.0016	0.054	0.108
3.81 (1.5)	30.84	28.89	0.051 (0.02)	0.0015	0.052	0.104
4.06 (1.6)	31.38	29.51	0.051 (0.02)	0.0015	0.050	0.100
4.31 (1.7)	31.90	30.11	0.051 (0.02)	0.0014	0.048	0.096
4.57 (1.8)	32.40	30.68	0.051 (0.02)	0.0014	0.047	0.093
4.82 (1.9)	32.87	31.23	0.051 (0.02)	0.0013	0.045	0.090
5.08 (2.0)	33.33	31.77	0.051 (0.02)	0.0013	0.044	0.087
5.33 (2.1)	33.78	32.28	0.051 (0.02)	0.0012	0.042	0.085
5.59 (2.2)	34.20	32.78	0.051 (0.02)	0.0012	0.041	0.082

3.5 Results

The results are presented as wall pressure distribution along the test section wall. The equivalence ratio is determined from total fuel and air flows entering the test section. The accuracy of the equivalence ratio is within 5 %.

3.5.1 Effects of Heat Release

Figure 3.2 show the wall pressure distribution of the base and ramp supersonic injection combination. The base equivalence ratio was kept constant while the fuel from the ramp was increased. A base line with no combustion is shown for reference. The 0.008 equivalence ratio from the ramp indicated that there was essentially no fuel injected from this port. At $\phi_{\text{ramp}} = 0.23$ upstream interaction is noted and it advances as the fuel flow increases to $\phi_{\text{ramp}} = 0.31$. It is noted that there is a tendency for the pressure rise to reach 2.1 at the onset of upstream interaction. This is the value at which the flow at this Mach and stagnation temperature becomes thermally choked. At high equivalence ratios the flow accelerates beyond 10H indicating that this is the region where heat is released.

A similar pressure rise is noted when the base and downstream combination is used as shown in Figure 3.3. The onset of upstream interaction occurs at $\phi_{\text{downstream}} = 0.23$ to 0.27.

Again, upstream interaction appears to begin once the pressure has risen to 2.

3.5.2 Comparison of Injection Combinations

1. Base + Ramp vs. Base + Downstream

Figures 3.4-3.6 show comparisons of base + ramp vs. base and downstream. It can be seen in Figure 3.4 that even small differences in the ramp or downstream can produce a noticeable difference in pressure rise. In Figure 3.5, when the equivalence ratios are almost identical, the two injection configurations appear to produce the same level of heat release.

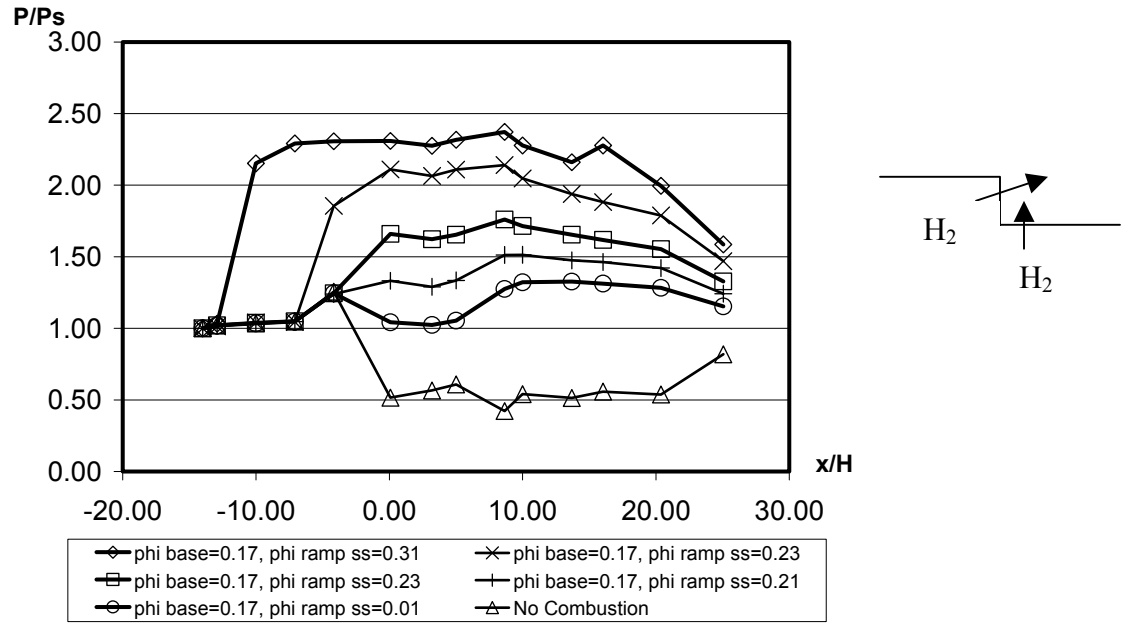


Figure 3.2-Pressure rise due to fuel injection in the base + ramp.

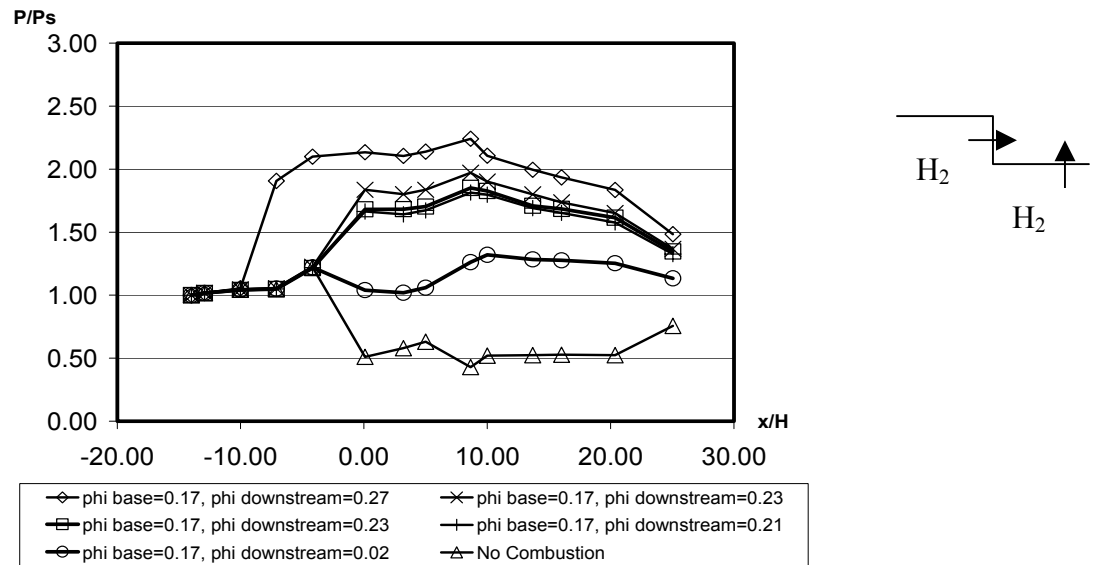


Figure 3.3-Pressure rise due to fuel injection in the base + downstream.

At higher equivalence ratios, Figure 3.6 shows that the ramp is more efficient than the downstream injection, possibly due to the entrainment of more fresh air from the core flow in the test section.

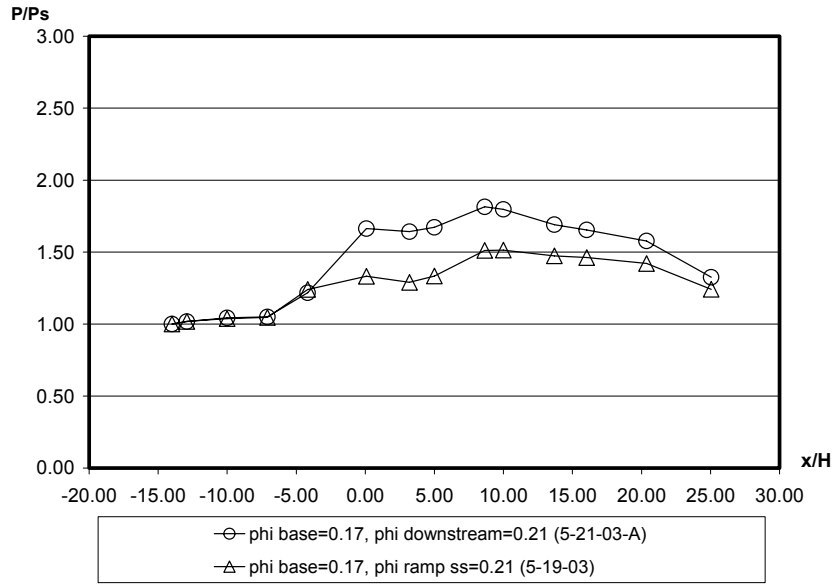


Figure 3.4-Comparison of the ramp ss and downstream injection sites with a base pilot.

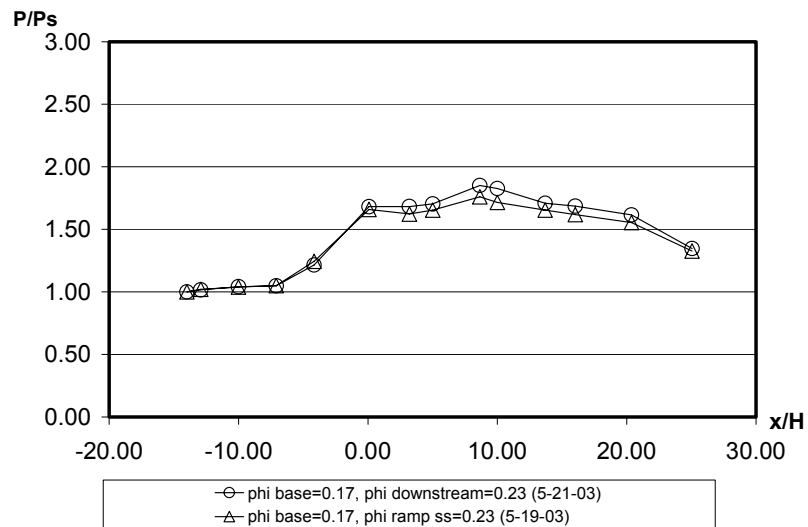


Figure 3.5-Comparison of the ramp ss and downstream injection sites with a base pilot.

2. Base + Ramp vs. Base + Downstream

Figure 3.7 shows a more efficient combination would be the base + ramp rather than base + downstream. Since the ramp injection occurs at the base of the ramp, in the subsonic recirculation region, it suggests that the fuel was used more efficiently at these equivalence ratios and some of the fuel injected from the downstream location left the combustion chamber unburned.

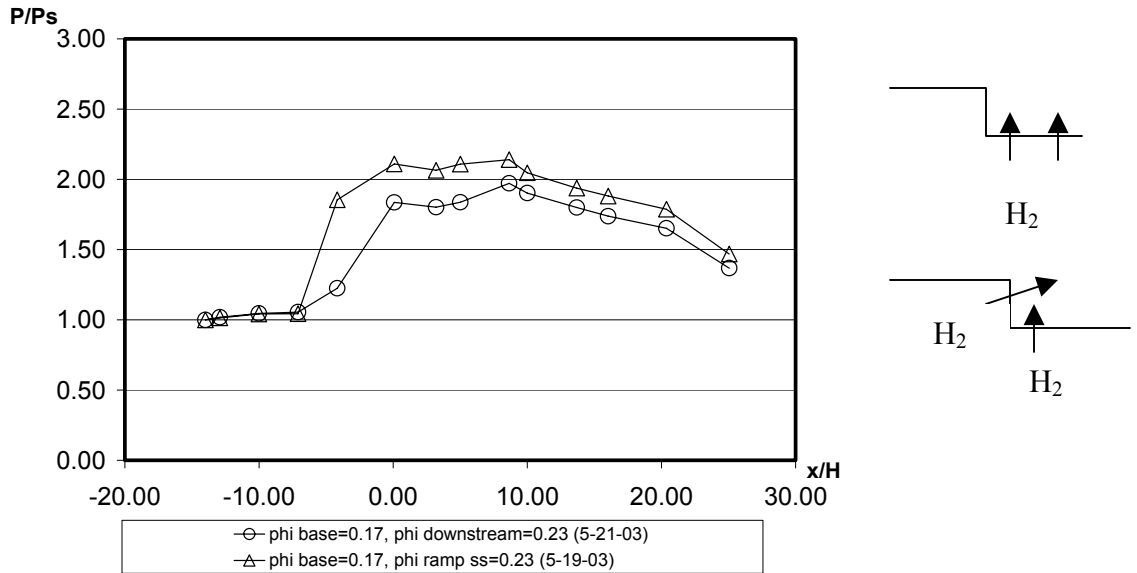


Figure 3.6-Ramp ss more efficient than the downstream injection site at high equivalence ratios.

3. Base + Ramp ss vs. Base + Upstream

A comparison of the ramp ss and upstream injection sites with a base pilot of $\phi=0.17$ was performed as shown in Figure 3.8. There is essentially no difference over this range of ϕ_{base} . However, when the base is used as a pilot only with most of the fuel provided from the other ports as shown in Figure 3.9, the upstream injection indicates significant pressure rise over the ramp. Most of this pressure rise is due to the shocks formed from the separation caused by the injection in the isolator. However, this effect is local due to the small size of the injectors and the speed of the flow entering the test section remains supersonic. The pressure rise in the combustion chamber can be attributed to increased efficiency due to partial premixing that occurs when fuel is injected upstream.

3.5.3 Comparison of Injection Configuration at Subsonic Conditions

Since part of the trajectory of the engine will operate at subsonic conditions, several tests were performed at $M < 1$ in the combustion chamber by lowering the air

stagnation pressure. Figure 3.10 shows ethylene injected only in the base. At equivalence ratios higher than 0.150, upstream interaction is noted. At higher equivalence ratio the large pressure jump is due both to increased heat release and to lowering the Mach number as the stagnation pressure was reduced. The drop in stagnation pressure is a result of the current facility controls.

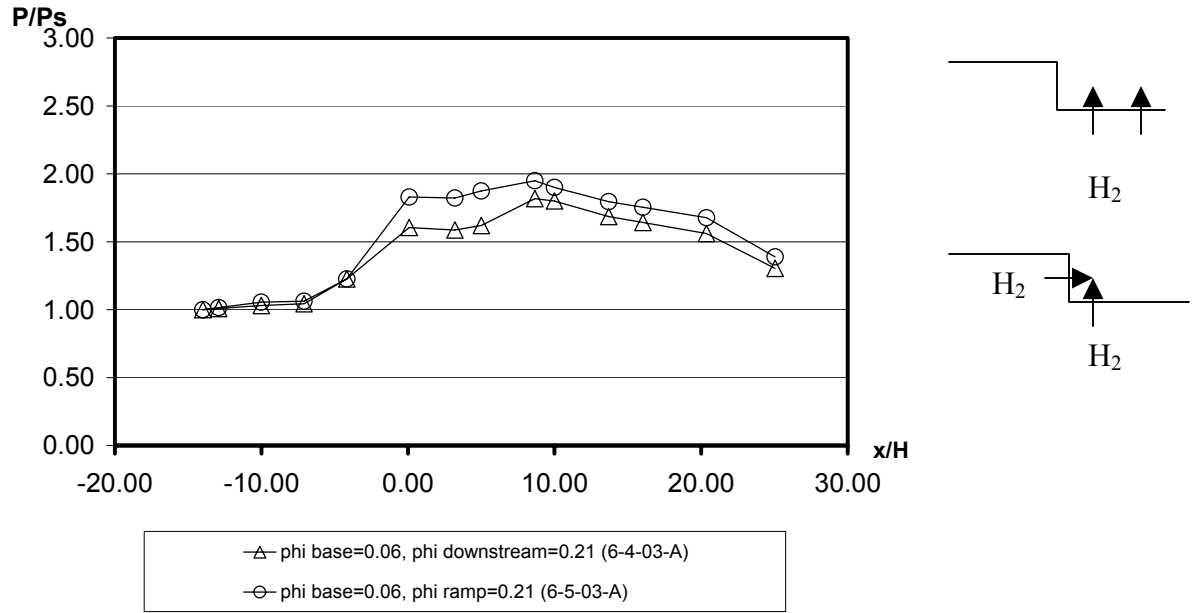


Figure 3.7- Downstream and ramp at comparable equivalence ratios.

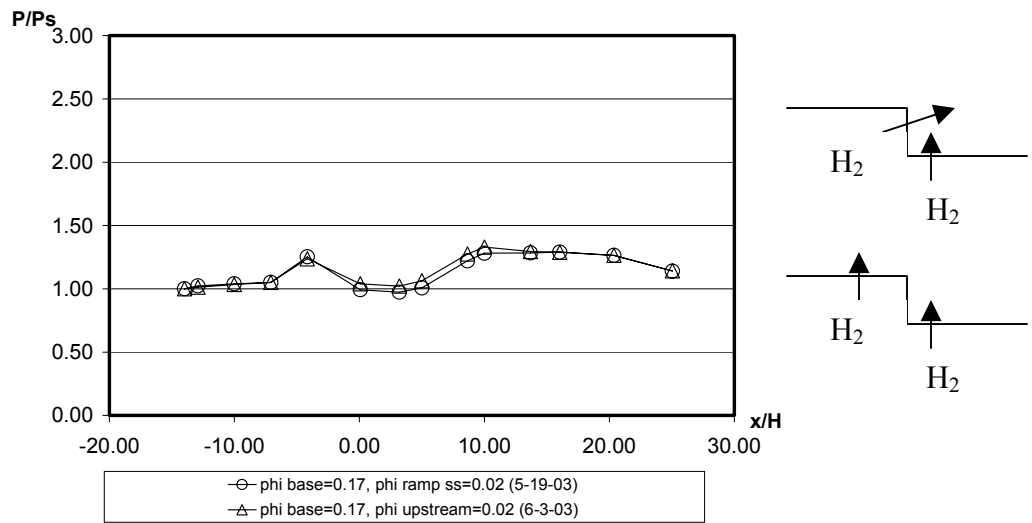


Figure 3.8-At low equivalence ratios, ramp ss and upstream injection sites showed no preferential gain in efficiency.

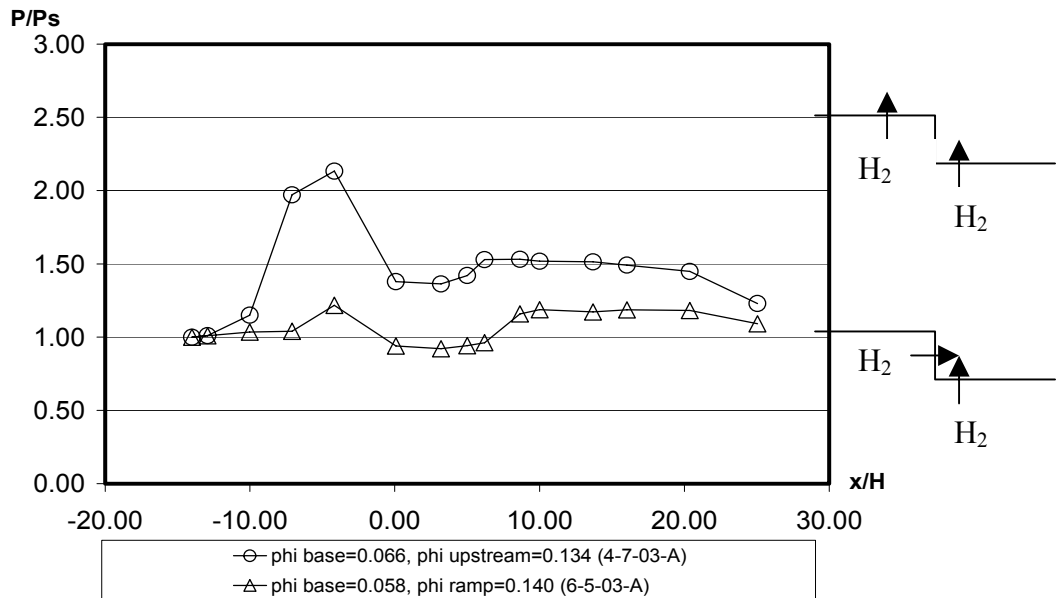


Figure 3.9- Upstream interaction was noted at $\phi=0.134$.

Ethylene was used in various injection combinations to investigate heat release efficiency. Injection was performed from three sites the upstream, base, and downstream. Tests revealed the following data for ethylene.

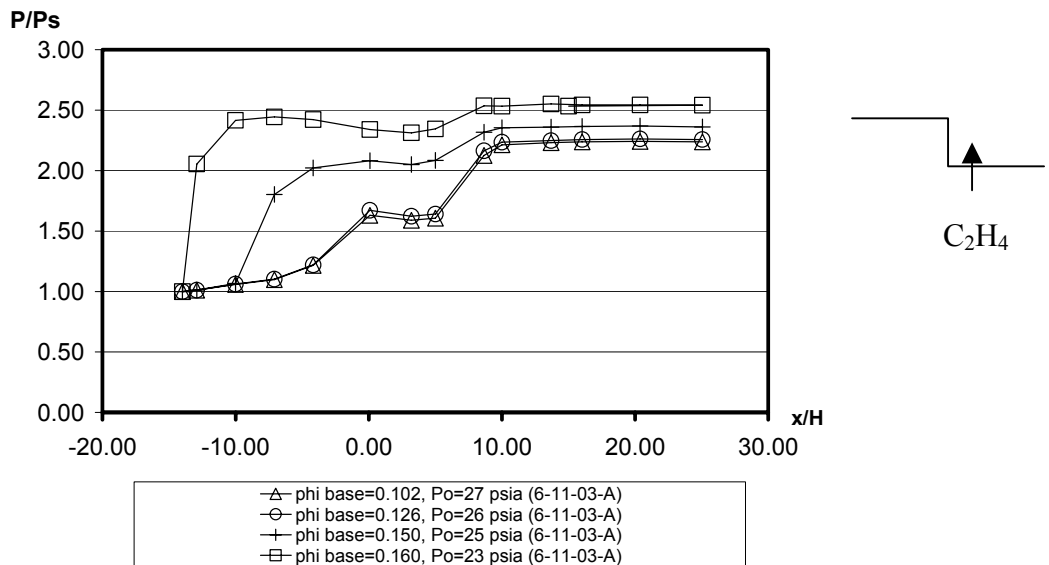


Figure 3.10- Ethylene injected in the base at low stagnation pressure.

1. Upstream + Ethylene Downstream

Ethylene injection downstream and hydrogen injection upstream at low stagnation pressure is shown in Figure 3.11. At higher ϕ_{upstream} , an increase in $\phi_{\text{downstream}}$ results in upstream interaction.

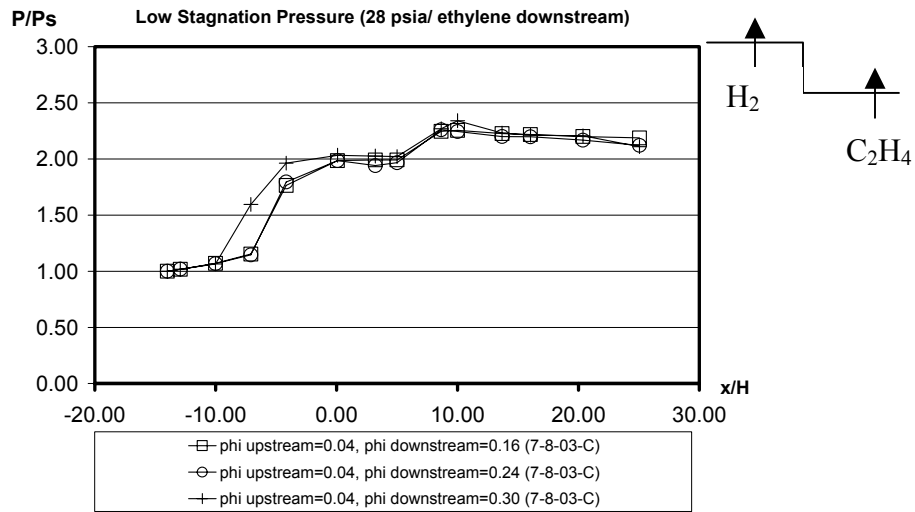


Figure 3.11- Ethylene injected downstream and hydrogen injected upstream at low stagnation pressure.

A subsequent test showing the repeatability of these effects at low stagnation pressures is shown in Figure 3.12. In this case the air stagnation pressure was lower than in Figure 3.11 which resulted in a higher level of normalized wall pressures. However, the distribution shows the same trend.

2. Upstream + Downstream vs. Upstream + Ramp

The Ethylene + Downstream vs. Ethylene-Ramp comparison shows a more efficient heat release from the downstream injector.

3. Upstream + Ethylene ramp ss + Downstream vs. Upstream + Ethylene Ramp

Figure 3.14 displays a low stagnation pressure comparison of ethylene injection at ramp ss + downstream and ramp, both with hydrogen injection upstream. The downstream injection is more efficient than the ramp injection at a $\phi = 0.15$ at both

locations. Both cases show thermal choking and upstream interaction indicating a definite limit in fueling.

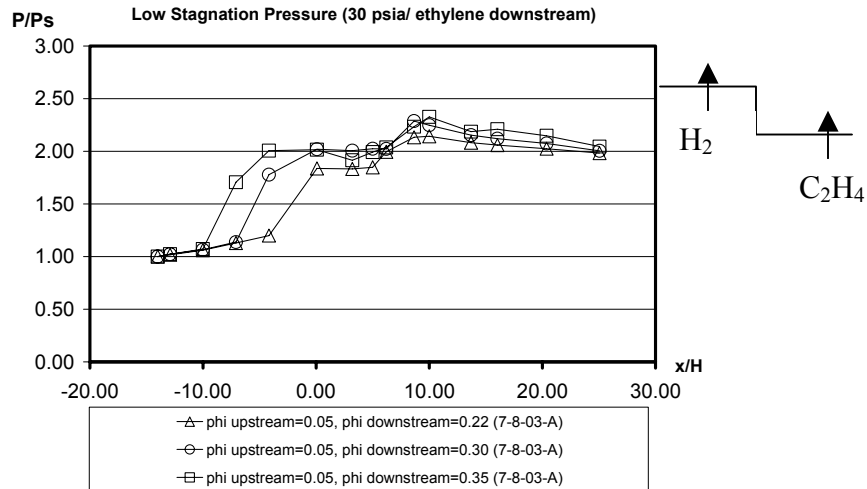


Figure 3.12- Ethylene injected downstream and hydrogen injected upstream at low stagnation pressure.

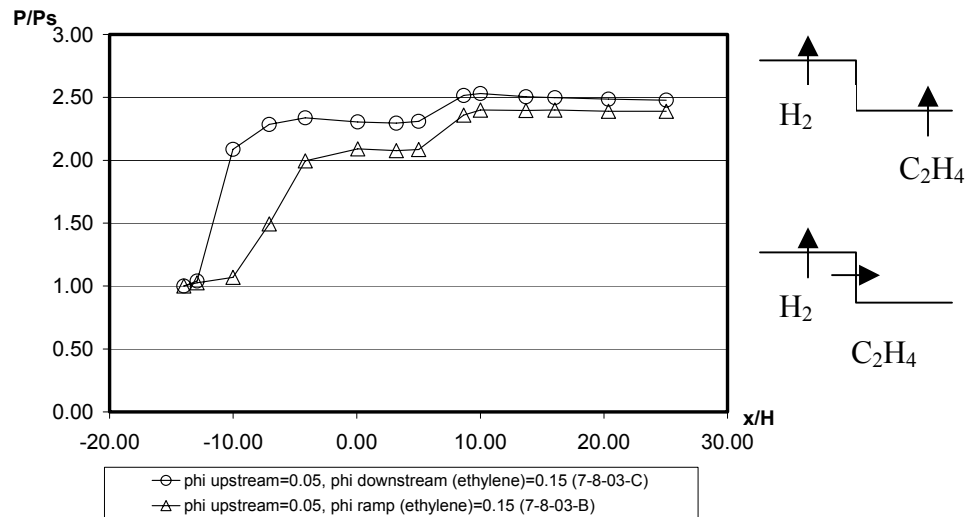


Figure 3.13- Comparison of downstream vs. ramp ethylene injection with upstream hydrogen pilot

3.5.4 Fuel Effects

Figure 3.15 compares ethylene and hydrogen heat release for a given injection configuration including upstream and base injection. In both cases hydrogen is injected from the base and the upstream injection changes from hydrogen to ethylene. A wall pressure distribution with hydrogen base injection only is shown for comparison.

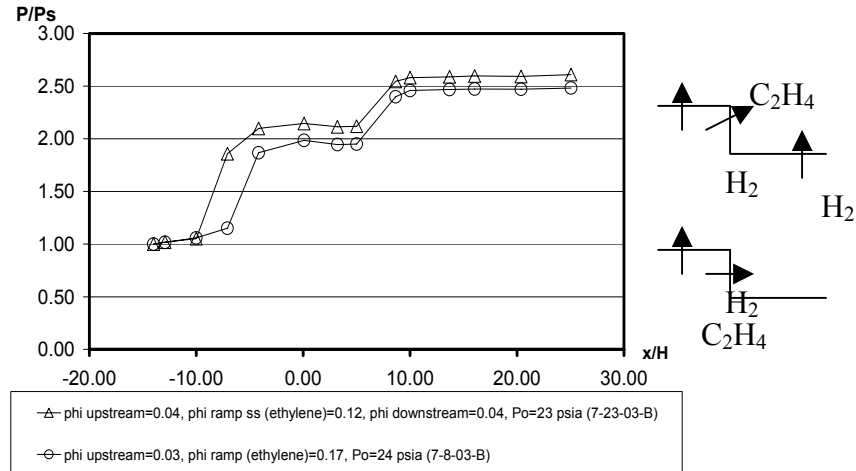


Figure 3.14- Low stagnation pressure comparison of ethylene injection at ramp ss + downstream and ramp, both with hydrogen injection upstream.

When upstream hydrogen is added the wall pressure increases as shown due to heat release. This effect is noticed immediately behind the step. When ethylene replaces hydrogen in the upstream injection there is no noticeable effect until 5H. After 5H, the pressure rise indicates that the ethylene injected upstream is burning. This delay in burning can be attributed to the longer timescale of combustion for ethylene. Hydrogen injected upstream at comparable equivalence ratios exhibits a higher pressure rise when contrasted with ethylene indicating higher combustion efficiency.

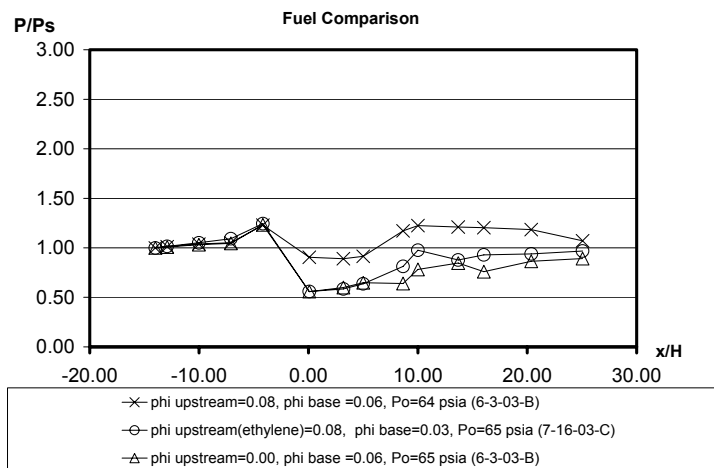


Figure 3.15- Ethylene vs. hydrogen injection with base hydrogen pilot

CHAPTER 4 SUMMARY OF RESULTS

This study examined the heat release of hydrogen and ethylene fuel injection at Mach 1.6 in a combination of fuel injection configurations and different gaseous fuels. An evaluation of the fuels at subsonic conditions in the combustor was also included.

The results indicated the following conclusions:

- Injection into the re-circulation region proved more efficient than alternate schemes due longer residence in this region.
- At low equivalence ratios there was no preferential injection in the combinations tested.
- At high equivalence ratios the supersonic ramp injection was more efficient than the subsonic injection.
- Upstream interaction is a limiting factor at high equivalence ratios and appears at these stagnation conditions for total equivalence ratios as low as $\phi_{\text{total}}=0.150$.
- The pressure reaches 2.1 at the onset of upstream interaction.
- Upstream injection has a strong tendency to produce upstream interactions when injected in large amounts, or in combination with test section $\phi > 0.2$.
- Injection from the supersonic ramp location seemed more efficient than the downstream location at high equivalence ratios due to enhanced fresh air entrainment.
- At equivalence ratios above 0.150, ethylene injected through the base produced upstream interactions.

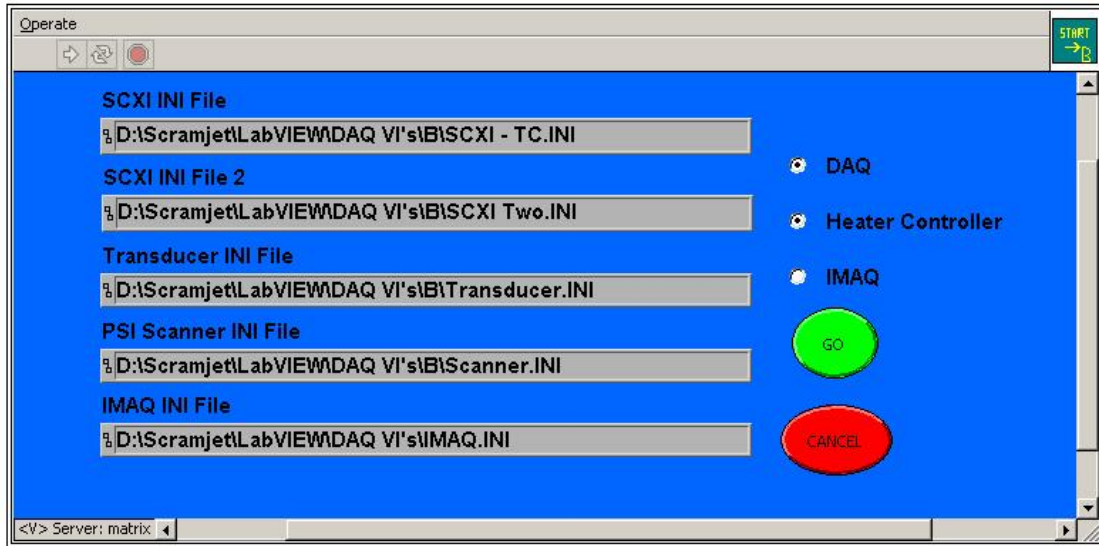
APPENDIX A DATA ACQUISITION AND CONTROL SOURCE CODE

The DAQC software was written in the LabVIEW (version 5.1) graphical environment developed by National instruments. LabVIEW is based on the G programming language employing graphical representations of program elements such as arithmetic and Boolean operators, loops, data structures, etc. In LabVIEW, programs are called virtual instruments (VI's) and sub-programs are called sub-VI's. Each VI or sub-VI has a front panel for program input and output and a block diagram containing the source code.

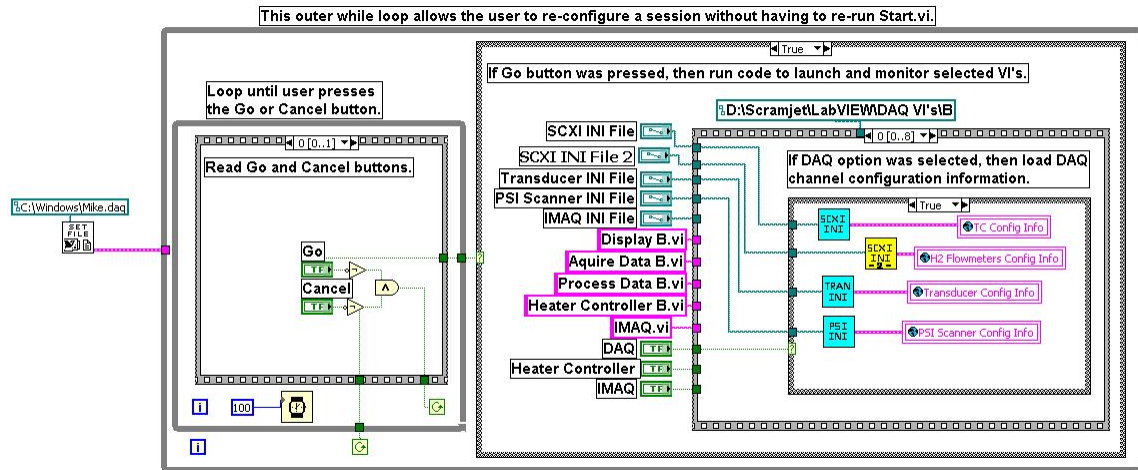
Presented below are both the front panels and block diagrams for the DAQC software written for this project. The six primary modules, Start-B.vi, Acquire B.vi, Process.vi, Display B.vi, Heater B.vi, and IMAQ.VI are given first. The sub-VI's called by these modules are then given in alphabetical order. Source code included with the LabVIEW package is not included. Also, empty Cases and Cases where the data is passed through unchanged are not included. The front panels and block diagrams are scaled to fit the page. The scaling is different for each VI shown. However, the scaling within each block diagram is the same.

Start-B

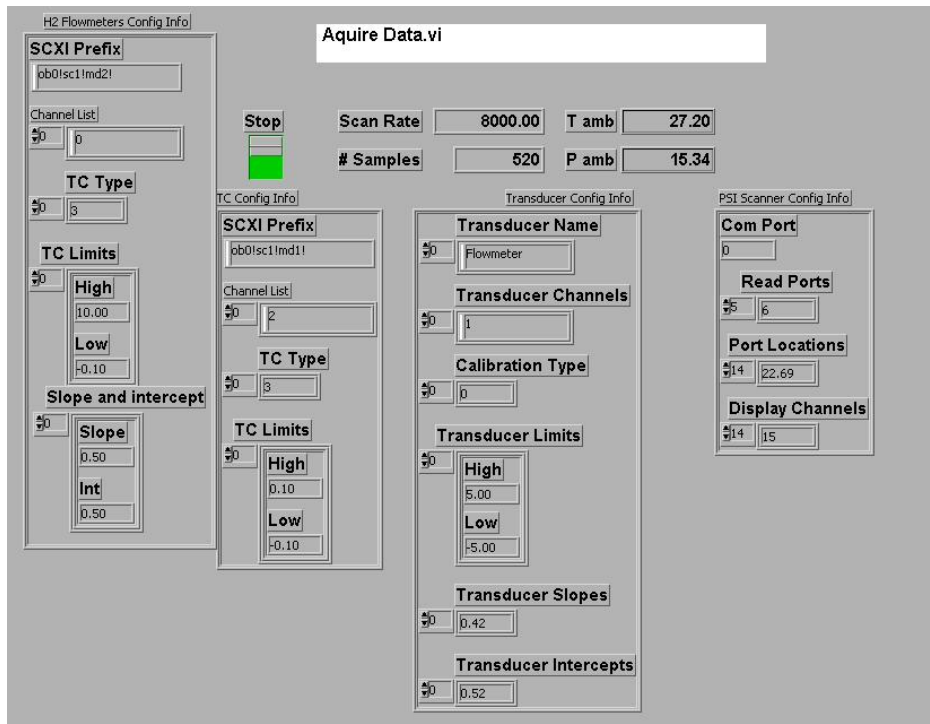
Front Panel



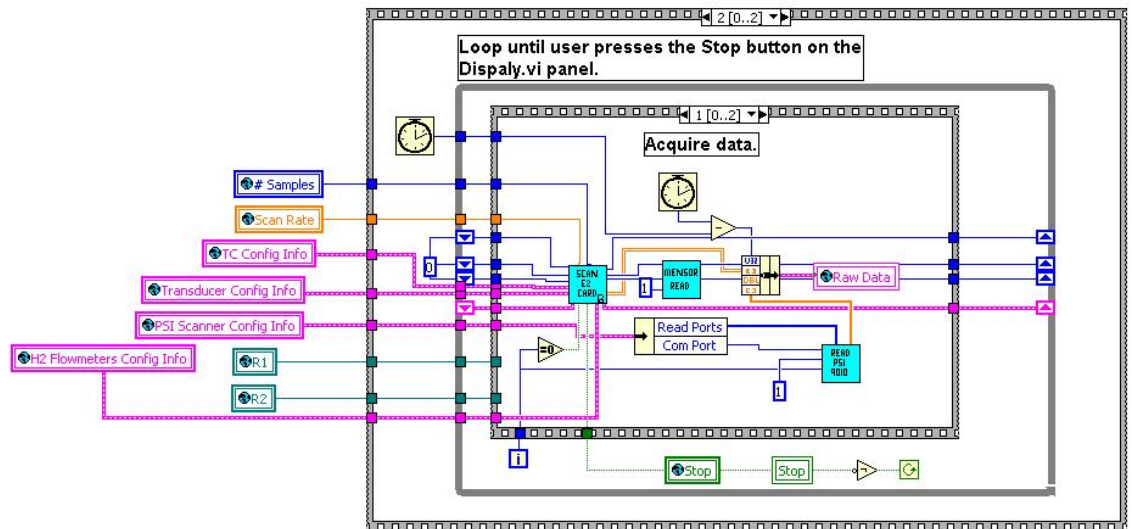
Block Diagram



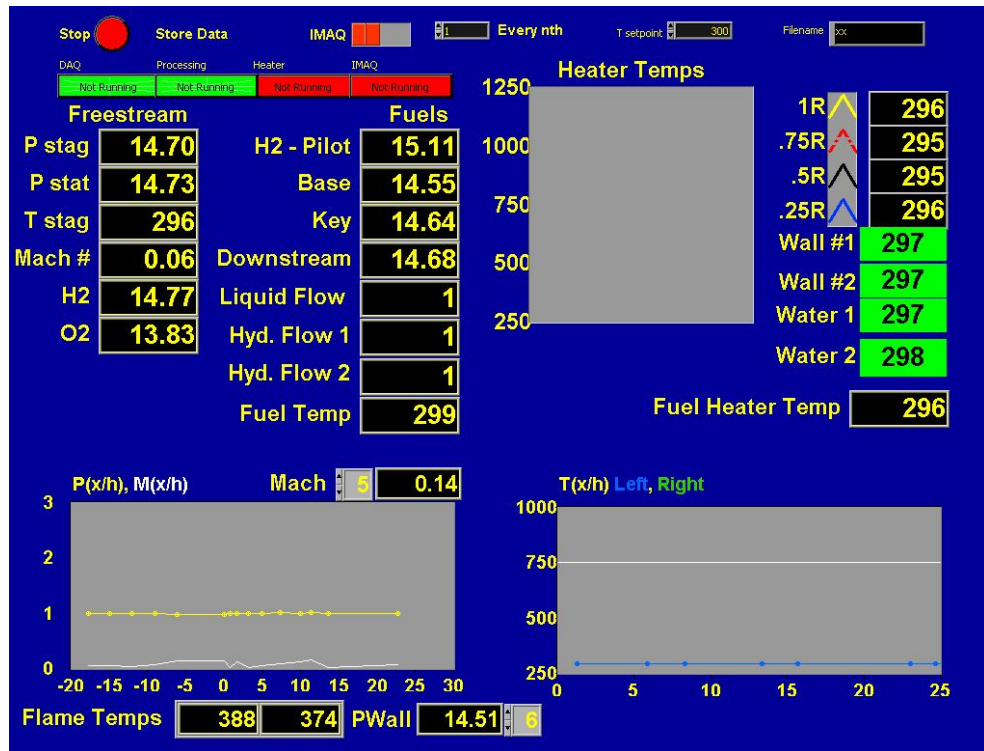
Aquire Data B



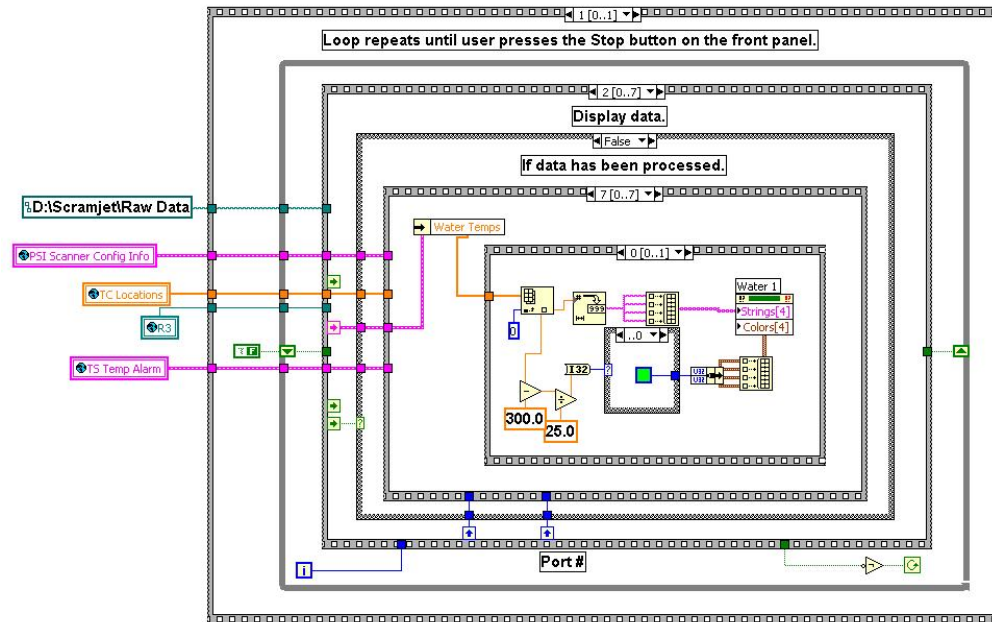
Block Diagram



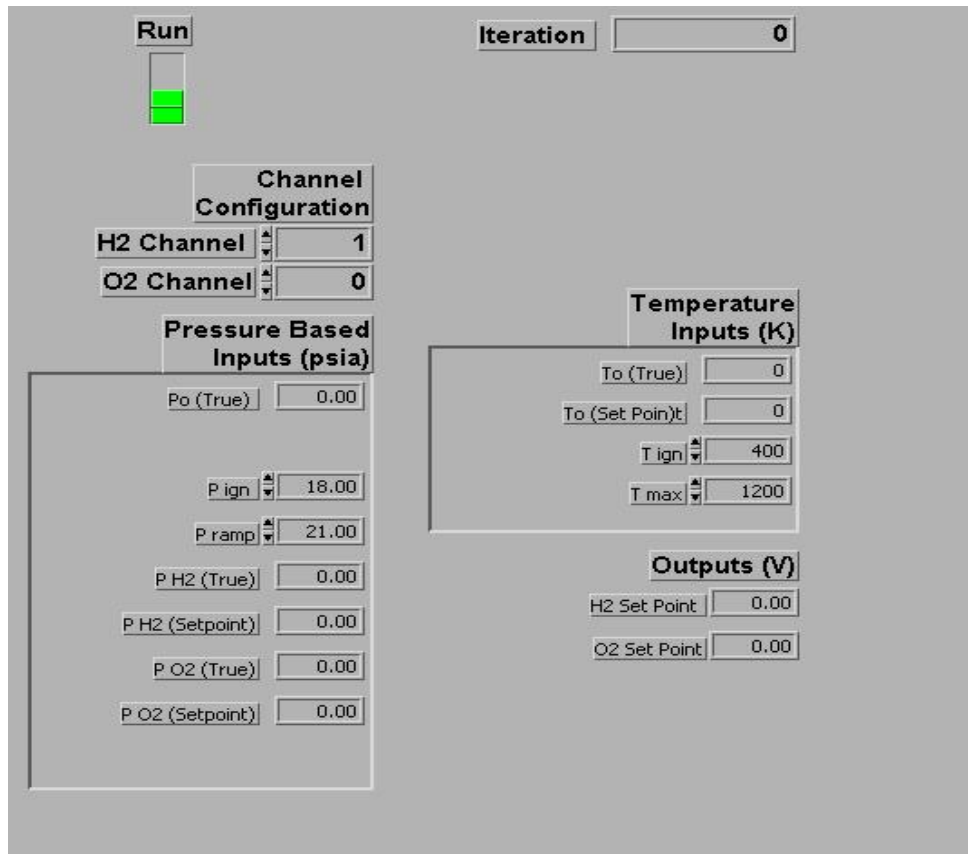
Display B



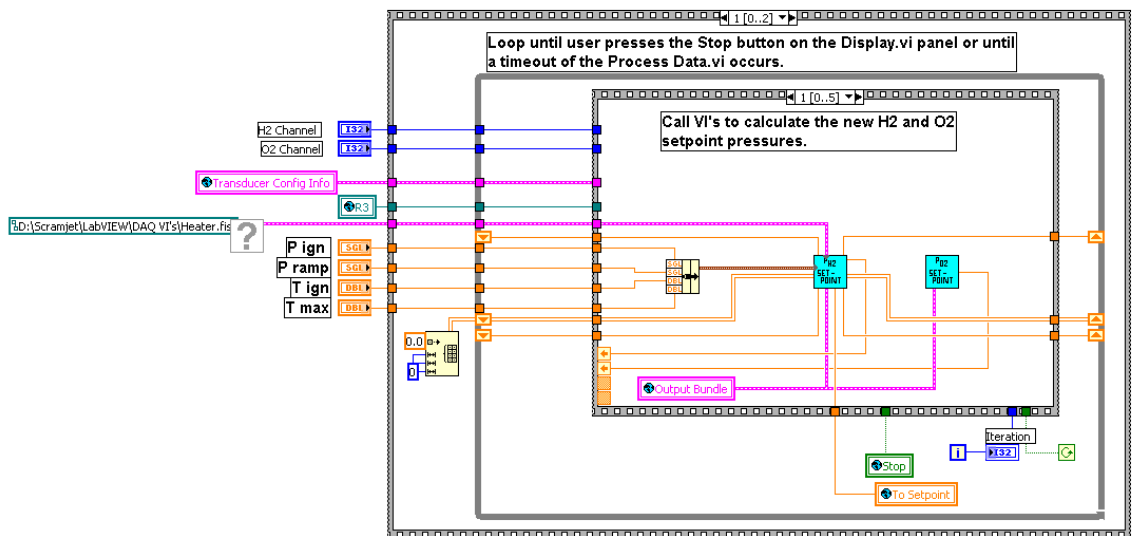
Block Diagram



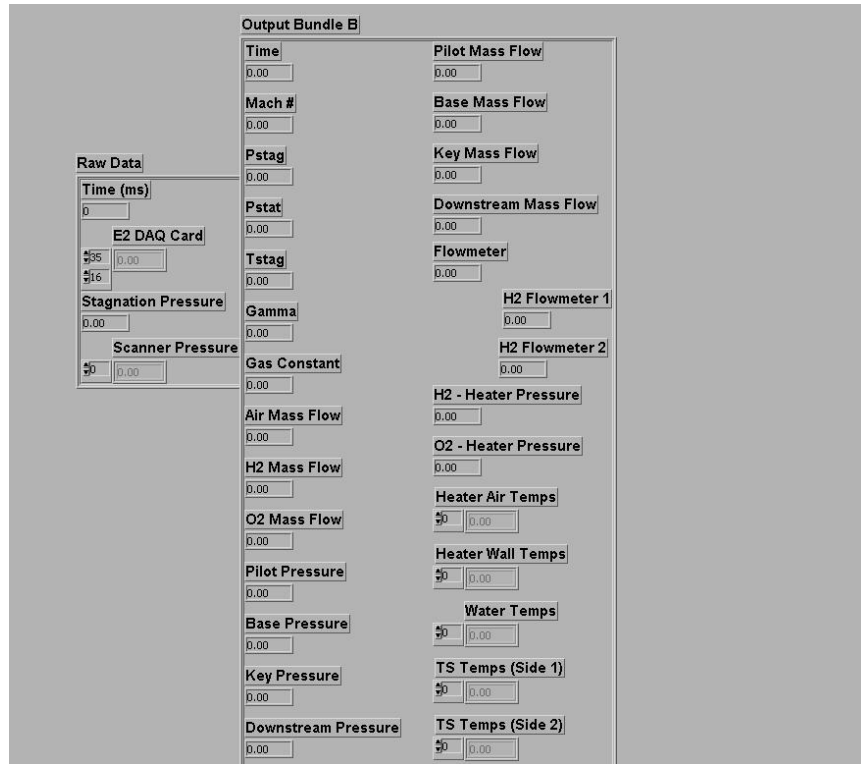
Heater Controller B



Block Diagram

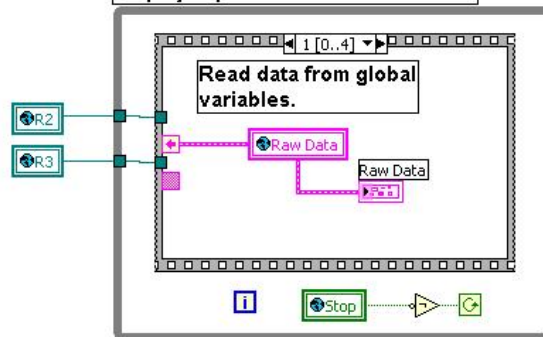


Process Data B

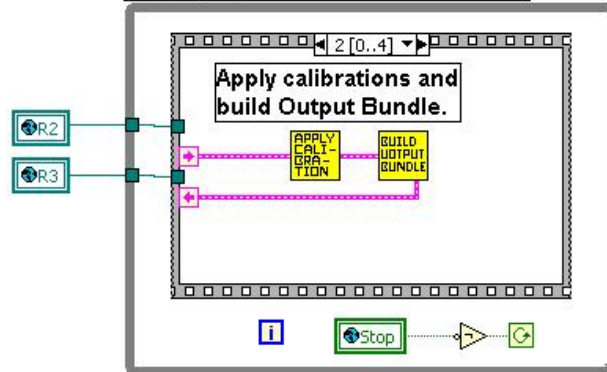


Block Diagram

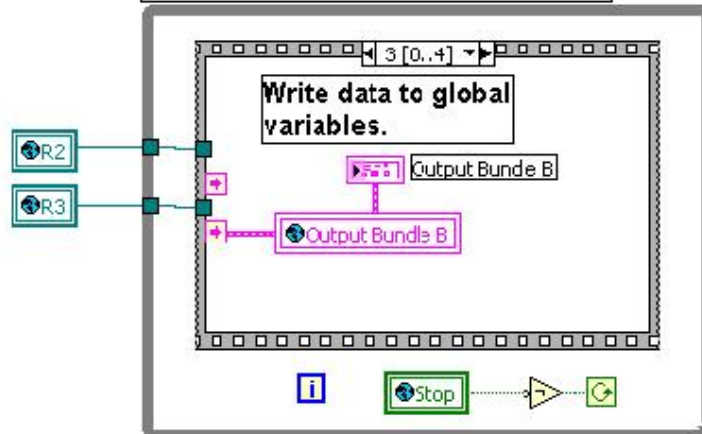
Main loop that iterates until the user presses the Stop button on the Display.vi panel.



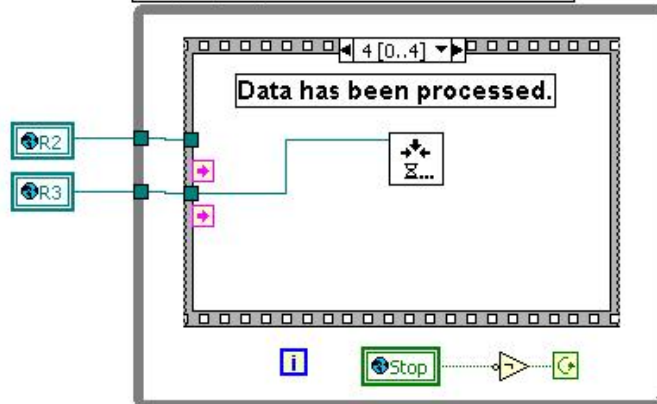
Main loop that iterates until the user presses the Stop button on the Display.vi panel.



Main loop that iterates until the user presses the Stop button on the Display.vi panel.



Main loop that iterates until the user presses the Stop button on the Display.vi panel.



APPENDIX B TEST MATRIX

The table presents the experiments conducted with hydrogen and ethylene, ethylene and a hydrogen and ethylene combination of fuels.

Number	Fuel	Po air (psia)	Injection Equiv. Ratio					Test number
			Upstream	Ramp super	Ramp	Base	Downstream	
1	Hydrogen	20-25	-	-	-	0.093	-	2-11-03-C
2	Hydrogen	20+	0.033	-	-	0.015	-	2-11-03-D
3	Hydrogen	20+	0.033	-	-	0.020	-	2-11-03-E
4	Hydrogen	34	-	-	-	0.092	-	2-25-03-C
5	Hydrogen	33	0.052	-	-	0.015-0.051	-	2-25-03-D
6	Hydrogen	26	-	-	-	0.150	-	3-18-03-A
7	Hydrogen	32.7	0.051	-	-	-	-	3-18-03-B
8	Hydrogen	35-38	-	-	-	0.110	-	3-18-03-C
9	Hydrogen	60-65	-	-	-	0.137	-	3-24-03-A
10	Hydrogen	60-65	0.138	-	-	0.066	-	4-7-03-A
11	Hydrogen	66	-	0.062	-	0.045	-	5-16-03-A
12	Hydrogen	60-66	0.171	-	0.412	-	-	5-16-03-B
13	Hydrogen	65	-	0.306	-	0.170	-	5-19-03-A
14	Hydrogen	65	-	-	-	0.172	0.265	5-21-03-A
15	Hydrogen	65	0.080	-	-	0.026-0.175	-	6-3-03-A
16	Hydrogen	65	0.082	-	-	0.059	-	6-3-03-B
17	Hydrogen	64	-	-	-	0.035-0.063	0.057-0.263	6-4-03-A
18	Hydrogen	63	-	-	0.059-0.212	0.056-0.059	-	6-5-03-A
19	Ethylene	24	-	-	-	0.155	-	6-11-03-A
20	Ethylene	18	-	-	0.286	-	-	6-11-03-B
21	Ethylene	20-27	0.456	-	-	0.128	-	6-11-03-C
22	Ethylene	19-25	0.051	-	-	0.119	-	6-11-03-D
23	Ethylene	19	-	-	-	0.064-0.130	0.045	6-12-03-A
24	Ethylene	17-37	0.041-0.168	-	-	-	0.027-0.153	6-12-03-B
25	Ethylene	20	-	-	-	0.166	0.144	6-12-03-C
26	Ethylene+H ₂	30	0.050 (H ₂)	-	-	-	0.373 (C ₂ H ₄)	7-8-03-A
27	Ethylene+H ₂	24-30	0.048 (H ₂)	-	0.234 (C ₂ H ₄)	-	-	7-8-03-B
28	Ethylene+H ₂	15-28	0.044 (H ₂)	-	-	-	0.355 (C ₂ H ₄)	7-8-03-C
29	Ethylene+H ₂	30-63	-	-	0.023 (C ₂ H ₄)	0.045 (H ₂)	-	7-16-03-A
30	Ethylene+H ₂	33-65	-	-	0.024 (C ₂ H ₄)	0.043 (H ₂)	-	7-16-03-B
31	Ethylene+H ₂	65	0.083 (C ₂ H ₄)	-	-	0.031 (H ₂)	-	7-16-03-C
32	Ethylene+H ₂	36	0.046-0.186 (C ₂ H ₄)	-	-	0.068-0.103 (H ₂)	-	7-16-03-D
33	Ethylene+H ₂	61	-	-	-	0.033 (H ₂)	0.319 (C ₂ H ₄)	7-17-03-A
34	Ethylene+H ₂	31	-	-	-	0.048 (H ₂)	0.42 (C ₂ H ₄)	7-17-03-B
35	Ethylene+H ₂	60-65	0.012-0.084 (C ₂ H ₄)	-	-	0.042-0.107 (H ₂)	0.032-0.161 (C ₂ H ₄)	7-17-03-C
36	Ethylene+H ₂	26-45	0.011 (C ₂ H ₄)	-	-	0.066 (H ₂)	0.108 (C ₂ H ₄)	7-21-03-A
37	Ethylene+H ₂	60-65	-	0.112-0.297 (C ₂ H ₄)	-	0.027-0.062 (H ₂)	0.097-0.284 (C ₂ H ₄)	7-21-03-B
38	Ethylene+H ₂	60-65	-	-	-	0.028 (H ₂)	0.041-0.174 (C ₂ H ₄)	7-22-03-A
39	Ethylene+H ₂	19	0.039 (H ₂)	0.171 (C ₂ H ₄)	-	-	0.065 (H ₂)	7-23-03-A
40	Ethylene+H ₂	26-41	0.132 (H ₂)	0.053-0.383 (C ₂ H ₄)	-	-	0.020-0.113 (H ₂)	7-23-03-B

APPENDIX C HYDROGEN FLOWMETER CALIBRATION

A two wire loop powered analog transmitter designed to linearly convert a frequency input to an equivalent 4-20 mA current output is incorporated with a turbine flowmeter. A current representation proportional to a flow is obtainable. A full-scale frequency range of 100 Hz- 10 KHz is selectable.

The Omega FTB-900 hydrogen flowmeter was calibrated according to the following procedures:

- Connect multimeter positive lead to power supply positive, negative lead to J1-3 as in schematic. Set multimeter to mA DC.
- Connect power supply negative lead to 250 ohm resistor; connect other resistor leg to J1-5.
- Connect frequency generator positive and negative leads to J1-12; respectively. Set output to sine wave & amplitude to zero.
- Set S1 for desired frequency range
- Turn power supply & frequency generator 'ON', multimeter should indicate approximately 4.00mA
- Adjust 'ZERO' (R25) for 4.00mA multimeter indication (record data)
- Set 'Sensitivity' adjust (R1) fully clockwise
- Adjust signal amplitude of frequency generator to 50mv & frequency to maximum desired point (full scale frequency)(record data)

- Adjust 'SPAN' (R19) for 20.00mA multimeter indication (record data)
- Reduce signal amplitude of frequency generator to zero, adjust 'ZERO' (R25) for 4.00mA multimeter indication if necessary.
- Adjust signal amplitude of frequency generator to 50mv, adjust 'SPAN' (R19) for 20.00mA multimeter indication if necessary
- Adjust frequency of frequency generator to exactly 50% of maximum frequency point in step H, multimeter should indicate 12.00mA +/- .06.
Repeat for 25% & 75% full-scale frequencies (record data)

Incorporate the following formula to check linearity at any frequency point.

$$\left(\frac{f}{f_{\max}} \times 16\right) + 4 = \text{mA}, \text{ where } f = \text{Flow rate frequency in Hz, } f_{\max} = \text{Frequency}$$

in HZ at which 20mA is set.

The above procedure results in these values:

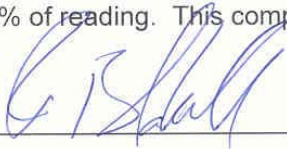
W/O #: 39342
 MODEL #: SPO5/8-MB-PH7-A-4RFX
 CALIBRATION GAS: HYDROGEN

P.O.#: 80045
 S/N: 231460
 DATE: 14-Aug-03

ACTUAL CUBIC FEET/MINUTE
 HYDROGEN @ 200 PSI & 70 DEG F

#	FREQ (Hz)	FLOW RATE	
		ACFM	PUL/ACF
1	1791.386	16.0830	6683.033
2	1483.994	13.5610	6565.862
3	1054.941	10.3180	6134.570
4	873.581	8.7170	6012.949
5	729.645	7.4130	5905.672
6	614.191	6.3620	5792.436
7	568.113	5.9400	5738.525
8	506.976	5.4380	5593.714
9	341.876	3.7820	5423.749
10	261.454	2.9510	5315.926
11	15.110	1.8150	4999.537
12			
13			
14			
15			
16			
17			
18			
19			
20			

The instrument referenced above was calibrated using standards traceable to the National Institute of Standards and Technology. The volumetric flowrates reported are within an uncertainty of +/- 0.10% of reading. This complies with MIL-STD-45662A.

Certified by:  Date: 8/14/03

LIST OF REFERENCES

1. Curran, E. T., Murthy, S.N.B., "Introduction," *High-Speed Flight Propulsion Systems*, Progress in Astronautics and Aeronautics, vol. 137, American Institute of Aeronautics and Astronautics, Washington DC, 1991, pp. 1-20.
2. Owens, Michael, "Effects of Mixing Schemes on Kerosene Combustion in a Supersonic Airstream," University of Florida Technical Report, January 1999.
3. Anderson, John, *Modern Compressible Flow*, 3rd Edition, McGraw Hill, New York, 2003.
4. Hill, Philip, and Peterson, Carl, *Mechanics and Thermodynamics of Propulsion*, 2nd Edition, Addison-Wesley, New York, 1992.
5. Heiser, William H., and Pratt, David T., *Hypersonic Airbreathing Propulsion*, American Institute of Aeronautics and Astronautics, Washington DC, 1994, pp. 507-512.
6. Anonymous, *U. S. Standard Atmosphere*, 1976, U. S. Government Printing Office, Washington, DC, 1976.
7. Magre, P., Sabelnikov, V., "Self Ignition of Hydrogen- Ethylene Mixtures in a Supersonic Airflow," AIAA Paper 02-5205, ONERA, 2002.
8. Sakima, Fuminori, Fei, He, "Interaction Phenomena Between a Supersonic cross Flow and a Transverse Sonic Jet," AIAA Paper 02-5187, 11th AIAA International Space Planes and Hypersonic Systems and Technologies Conference, Orleans, France, September 2002.
9. Muruganandam, T.M., Lakshmi, Srihari, "Mixing of Transversely Injected Jets into a Cross Flow Under Low- Density Conditions," AIAA Paper 00-0203, 38th AIAA Aerospace Sciences Meeting, Reno, Nevada, January 2000.
10. Tien, J.H., Stalker, R.J., "Release of Chemical Energy by Combustion in a Supersonic Mixing Layer of Hydrogen and Air," *Combustion and Flame* 130:329-348, 2002.
11. Gruber, M. R., Nejad, A. S., Chen, T. H., and Dutton, J. C., "Mixing and Penetration Studies of Sonic Jets in a Mach 2 Freestream," *Journal of Propulsion and Power*, vol. 11, no. 2, March-April 1995, pp. 315-323.

12. Papamoschou, Dimitri, "Mixing Enhancement Using Axial Flow," AIAA Paper 00-0093, 38th AIAA Aerospace Sciences Meeting, Reno, Nevada, January 2000. Lourdes, Maurice, Edwards, Tim, *Liquid Hydrocarbon Fuels For Hypersonic Propulsion for High-Speed Flight Propulsion Systems*, Progress in Astronautics and Aeronautics, vol. 189, American Institute of Aeronautics and Astronautics, Washington DC, 2000, pp. 757-822.
13. Heiser, W.H., Pratt, D.T., "Aerothermodynamics of the Dual-Mode Combustion System," Progress in Astronautics and Aeronautics, vol. 189, American Institute of Aeronautics and Astronautics, Washington DC, January 2000, pp. 569-595.
14. Cockrell, C.E., Auslender, A.H., Guy, R.W., McClinton, C.R., Welch, S.S., "Technology Roadmap for Dual-Mode Scramjet Propulsion to Support Space-Access Vision Vehicle Development," 11th AIAA International Space Planes and Hypersonic Systems and Technologies Conference, Orleans, France, September 2002.
15. Murthy, S.N.B., "Basic Performance Assessment of Scram Combustors," *High-Speed Flight Propulsion Systems*, Progress in Astronautics and Aeronautics, vol. 137, American Institute of Aeronautics and Astronautics, Washington DC, 1991, pp. 597-695.
16. Gregory, David C., Han, Sam, "Effects of Multiple Flows on Ejector Performance in an Ejector-Ramjet Rocket Engine," *Journal of Propulsion and Power*, vol. 18, no. 3, May-June 2002, pp. 592-599.
17. Daines, Russell, Segal, Corin, "Combined Rocket and Airbreathing Propulsion Systems for Space Launch Applications," *Journal of Propulsion and Power*, vol. 14, no.5, Sept.-Oct.1998, pp. 605-612.
18. Kepler, C., Champagne, G., "Performance potential of Air Turbojet Employing Supersonic Through Flow Fan," AIAA paper 89-0010, January 1989.
19. Mavris, Dimitri, "Pelegrine Hypersonic Strike Fighter Weapons System," *Proposal to AIAA-Aerospace Systems Design Laboratory-GIT*, June 2002.
20. Czysz, P., Murthy, S.N.B., "Energy Analysis of High Speed Flight," *High-Speed Flight Propulsion Systems*, Progress in Astronautics and Aeronautics, vol. 137, American Institute of Aeronautics and Astronautics, Washington DC, 1991, pp. 143-236.
21. Anonymous, *Selected Properties of Hydrogen*, 1981, National Bureau of Standards- U.S. Department of Commerce, Washington D.C., 1981.
22. Baurle, R.A., Eklund, D.R., "Analysis of Dual Mode Hydrocarbon Scramjet Operation at Mach 4 – 6.5," 37th AIAA Joint Propulsion Conference, Salt Lake City, Utah, July 2001.

23. Waltrup, P. J., Stull, "Upper Bounds on the Flight Speed of Hydrocarbon-Fueled Scramjet-Powered Vehicles," *Journal of Propulsion and Power*, vol. 17, no.6, November-December 2001, pp. 1199-1204.
24. Choudhuri, Ahsan R., Gollahalli, S.R., "Stability of Hydrogen/ Hydrocarbon Blended Fuel Flames," *Journal of Propulsion and Power*, vol. 19, no.2, March-April 2003, pp. 220-225.
25. Sisco, J.C., Austin, B.L., "Ignition Studies of Hydrogen Peroxide and Kerosene Fuel," 41st AIAA Aerospace Sciences Meeting, Reno, Nevada, January 2003.
26. Owens, M., Segal, C., "Combustion of Kerosene in a Supersonic Airstream-Thermal Efficiency of Selected Injection Configurations," University of Florida Technical Report, May 1999.
27. Lewis, Mark, "Significance of Fuel Selection for Hypersonic Vehicle Range," *Journal of Propulsion and Power*, vol. 17, no.6, November-December 2001, pp. 1214-1221.
28. Ogorodnikov, Donat A., Vinogradov, Viacheslav A., "Russian Research on Experimental Hydrogen-Fueled Dual-Mode Scramjet: Conception and Preflight Tests," AIAA Paper 98-1586, 8th AIAA International Space Planes and Hypersonic Systems and Technologies Conference, Norfolk, Virginia, April 1998.
29. Sabelnikov, V.A., Penzin, "Scramjet Research and Development in Russia," *Scramjet Propulsion*, Progress in Astronautics and Aeronautics, vol. 189, American Institute of Aeronautics and Astronautics, Washington DC, June 2000, pp. 223-367.
30. Chinzei, Nobuo, Mitani, Tohru, Yatsuyanagi, Nobuyuki" Scramjet Engine Research at the National Aerospace Laboratory in Japan," *Scramjet Propulsion*, Progress in Astronautics and Aeronautics, vol. 189, American Institute of Aeronautics and Astronautics, Washington DC, June 2000, pp. 159-222.
31. Anonymous, "The Hyshot Flight Program," February 2003, www.mech.uq.edu.au/hyper/hyshot, December 8, 2003.
32. Paull, A., Stalker, R.J., "Scramjet Testing in the T4 Impulse Facility," AIAA 8th Space Planes and Hypersonic Systems and Technology Conference, Orleans, France, June 1998, pp. 1-9.
33. Bissinger, N.C., Koschel, W., "Scramjet Investigations Within the German Hypersonics Technology Program," *Scramjet Propulsion*, Progress in Astronautics and Aeronautics, vol. 189, American Institute of Aeronautics and Astronautics, Washington DC, 2000, pp. 119-158.
34. Owens, M., Segal, C., "Flame-Holding Configurations for Kerosene Combustion in a Mach 1.8 Airflow," *Journal of Propulsion and Power*, vol. 14, no.4, July-August 2003, pp. 456-461.

35. Owens, M., Mullagiri, S., Segal, C., Ortwerth, P.J., Mathur, A.B., "Thermal Choking Analyses in a Supersonic Combustor," *Journal of Propulsion and Power*, vol. 17, no.3, July-August 2003, pp. 611-616.
36. Brandstetter, A., Denis, S.R., Kau, H.P., "Flame Stabilization in Supersonic Combustion," AIAA paper 02-5224, January 2002.
37. Mathur, T., Jackson, K., Donbar, J., Donaldson, W., Jackson, T., "Supersonic Combustion Experiments with a Cavity-Based Fuel Injector," *Journal of Propulsion and Power*, vol. 17, no.6, Nov.-Dec. 2001, pp. 1305-1313.
38. Gousskov, O.V., Kopchenov, V.I., "Investigation of Ignition and Flame Stabilization Behind the Strut in a Supersonic Flow," AIAA Paper 02-5269, CIAM, 2002.
39. Kamel, M.R., Morris, C.I., Stouklov, I.G., "Imaging of Hypersonic Reactive Flow around Cylinders and Wedges," The Combustion Institute Paper 95F-196, 1995.
40. Yu, Ken, Wilson, Ken, Schadow, Klaus, "Effect of Flame-Holding Cavities on Supersonic Combustion," 35th AIAA Joint Propulsion Conference, June 1999.
41. Hojinacki, John T., "Ramjet Engine Fuel Injection Studies," Air Force Aero Propulsion Laboratory Technical Report AFAPL-TR-72-76, November 1972.

BIOGRAPHICAL SKETCH

Daniel F. Cuesta was born in Miami, Florida, on October 31, 1976. He seeks to continue his research interests in hypersonics.